A Novel 3D Printed Wrist Rehabilitation Robot: Design, Development and Optimal Trajectory Planning

Nima Amooye Foomany

A Thesis

in

The Department

of

Mechanical and Industrial Engineering

Presented in Partial Fulfillment of the Requirements

for the Degree of

Master of Applied Science (Mechanical Engineering) at

Concordia University

Montréal, Québec, Canada

October 2021

© Nima Amooye Foomany, 2021

CONCORDIA UNIVERSITY

School of Graduate Studies

This is to certify that the thesis prepared

By: **Nima Amooye Foomany**

Entitled: **A Novel 3D Printed Wrist Rehabilitation Robot:**

Design, Development and Optimal Trajectory Planning

and submitted in partial fulfillment of the requirements for the degree of

Master of Applied Science (Mechanical Engineering)

complies with the regulations of this University and meets the accepted standards with respect to originality and quality.

Signed by the Final Examining Committee:

_____ Chair
Dr. Farjad Shadmehri

_____ Examiner
Dr. Arash Mohammadi

_____ Examiner
Dr. Farjad Shadmehri

_____ Supervisor
Dr. Javad Dargahi

Approved by _____
Martin D. Pugh, Chair
Department of Mechanical and Industrial Engineering

_____ 2021

_____
Mourad Debbabi, Dean
Faculty of Engineering and Computer Science

Abstract

A Novel 3D Printed Wrist Rehabilitation Robot:
Design, Development and Optimal Trajectory Planning

Nima Amooye Foomany

Rehabilitation of patients suffering after stroke impairment is a lengthy process and requires experienced therapists. These limitations have led to the introduction of rehabilitation robots that can operate for a longer time while eliminating the lack of professional therapists. In this thesis, we propose a two-degrees-of-freedom robot for wrist rehabilitation, referred to as MOCH. The MOCH mechanism comprises a remote center of motion (RCM) mechanism with a rotation center outside of the robot structure. When the patient holds the robot end-effector, coinciding the RCM of the robot with the rotation axis of the wrist, allows pure rotational motion of the hand. As the RCM lies out of the robot structure, there is less risk of interference with the patient. Furthermore, MOCH benefits a novel actuation that enables the actuators to be grounded, reducing the inertia and the size of the robot. The optimal design of MOCH is provided considering the mechanical criteria and requirements of the wrist rehabilitation. Based on the proposed design, a prototype of the robot is developed with a total mass of 1.3 kg using 3D printing technology. Additionally, we introduce a novel methodology for passive rehabilitation exercise, exploiting the wrist dynamics which removes the complexity of force/impedance control approaches. This method involves designing an optimal trajectory within the limits of the wrist motion, and to keep the applied torque on the patient's hand in a safe range without using force sensors. The proposed trajectory is tested on a healthy individual using the implemented prototype.

Acknowledgments

During my study as a student in mechanical engineering at Concordia University, I gained a lot of knowledge, experiences, and skills which certainly will help me in the next steps of my life especially in finding a good job and even establishing my own company. I want to thank my supervisor Dr. Dargahi for his guidance during my study. A special thanks to my mentor and my best friend Amir Molaei who helped me a lot in both theoretical and practical parts of my project and this challenging path. I also would like to thank my parents Zahra and Hassan and my only sister Negin who encouraged me to keep going and never giving up on my study. Finally thanks to Concordia University and its staff for the good facilities, events, and classes which helped me a lot in this path.

Contents

List of Figures

List of Tables

Nomenclature

δ	Half length of the linear carriage
κ	Condition number
ϕ	Workspace variable for radial/ulnar
τ_ϕ	Torque of radial/ulnar motion
τ_θ	Torque of flexion/extension motion
θ	Workspace variable for flexion/extension
a	Distance between point H and lead screw axis
b	Length of BC
C^{eq}	Equality constraints
C^{ineq}	Inequality constraints
C_ϕ	Damping ratio of the human wrist in radial/ulnar direction
C_θ	Damping ratio of the human wrist in flexion/extension direction
d	Total length of the allowable lead screw stroke within the rotating arm
I_ϕ	Moment of inertia of the human wrist in radial/ulnar direction
I_θ	Moment of inertia of the human wrist in flexion/extension direction
J	Jacobian matrix

k_1	Gear ratio of lead screw and nut
k_2	Gear ratio of the rotating arm gear and pinion gear
K_ϕ	Stiffness ratio of the human wrist in radial/ulnar direction
K_θ	Stiffness ratio of the human wrist in flexion/extension direction
l	Length of CH
m	Length of BH
q_1	Angular rotation of servo motor 1
q_2	Angular rotation of servo motor 2
w	Objective function
x	Position of the slider from joint B

Chapter 1

Introduction and Literature Review

Stroke is one of the main causes of death and disability worldwide [1]. Currently, more than 80 million living individuals have experienced a stroke in their life and each year we have more than 13.7 million new cases [1]. Almost 5.5 million cases of these new cases lead to death and the rest face upper limb impairment [1]. It's been proved that doing rehabilitation therapy in the early stages after stroke has a major effect on treatment and recovery [2]. Rehabilitation therapy is a long time, repetitive procedure and it takes at least 6 months to show its effectiveness [2]. As rehabilitation therapy needs continuance and repetition to reach maximum recovery, it is an expensive service for patients and a burden on the health care system [3], [4]. For this reason, using robots for rehabilitation therapy services can be very useful. Robotics is playing a major role in the automation of many applications and rehabilitation therapy is not an exception. Since 30 years ago there has been an increasing approach in using robots in rehabilitation therapies.

One of the first and most famous robots designed and developed for upper limb rehabilitation is MIT-MANUS which has 5 DoF (degrees of freedom) [5]. The MANUS primary version was introduced in 1992 which is a SCARA planar mechanism with 2 DoF aiming shoulder and elbow motions. In 2007 a new version of MANUS was introduced by adding a wrist and forearm robot module with 3 DoF [6].

In 1999 a system named MIME was designed by Lum et al. for shoulder and elbow rehabilitation using a 6 DoF industrial PUMA serial robot [7], [8]. As shown in Fig. 1.1, the patient's hand is fixed in a splint which is connected to the robot end-effector and the interaction forces and torques

between the robot and patient are measured using a 6 axis sensor [9]. The positive effect of using MIME in rehabilitation therapy comparing to usual therapies was demonstrated in a clinical trial [9].

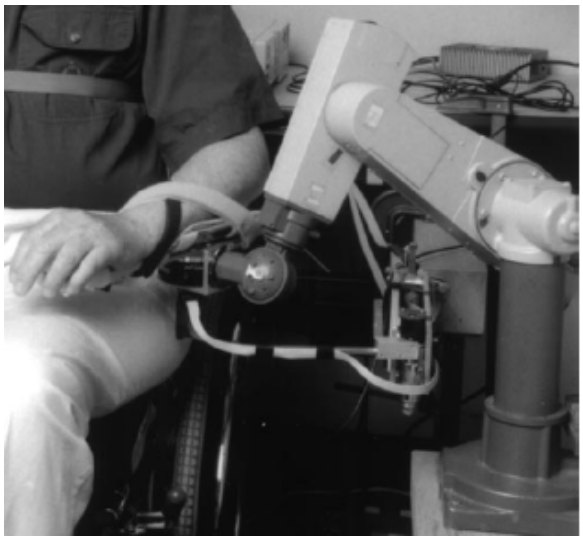

Figure 1.1: MIME system developed by Lum et al. [7].

In 2000 a robot called ARM Guide was introduced by Reinkensmeyer et al. [10]. As shown in Fig. 1.2, it aims to improve arm disabilities after brain injuries by moving the arm in a linear path [11].

Figure 1.2: ARM guide developed by Reinkensmeyer et al. [10].

In 2005 a 6 DoF robot named ARMin which aims at rehabilitation of arm impairment was introduced [12]. The robot is equipped with several position, speed, and torque sensors and is able to do four various control strategies [12]. Firstly, the rehabilitation process done by a professional therapist can be recorded, and then the robot can repeat it [12]. Secondly, the robot can do several defined trajectories on the patient [12]. Thirdly, for patients who can't move their hands, the robot can help them to do predefined movements [12]. Fourthly, when the patient moves his/her hand, the robot tries to estimate the forces and torques and does a portion of them to help the patient [12]. In 2007 by adding more degrees of freedom to ARMin, ARMin 2 was introduced which in comparison to the first version has more complicated maneuvers. ARMin 2 has 7 DoF which causes the patient to feel more comfortable during therapy [13]. Bi-Manu-Track is another rehabilitation device that has been developed especially for the forearm and wrist by Hesse et al. [14]. As Fig. 1.3 shows, it has a total of 2 DoF, which just covers one DoF for the wrist and the other one is reserved for the forearm [14].

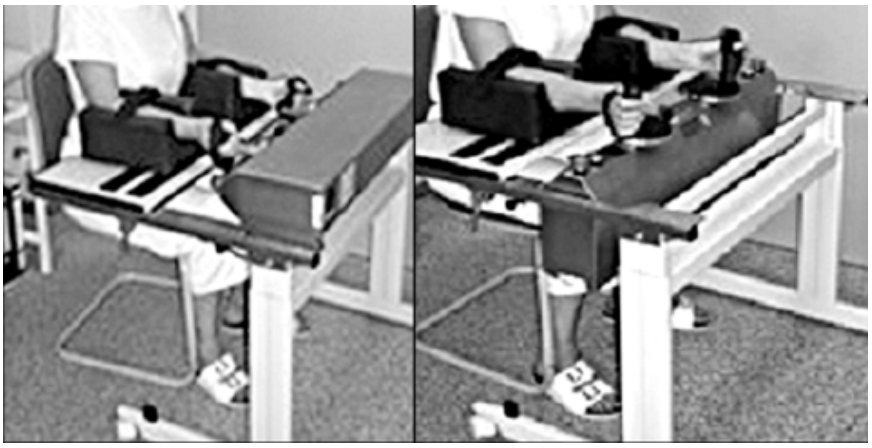

Figure 1.3: Bi-Manu-Trac developed by Hesse et al. [15].

The patient sits at a table with the device and his/her hand placed inside two ergonomic parts, strapped and fastened by bands. The therapist can adjust the angle, speed, and torque of rotation on a control panel [15]. Two types of handles were designed for the device which needs to be demounted and remounted to switch from flexion/extension to pronation/supination [15]. Simple structure and the ability to perform rehabilitation practice on both hands at the same time are good features of this device [15]. In a clinical test with 12 patients, motor functions improved even after a short period of

utilization of the robot [16]. A 4 DoF parallel robot named RiceWrist was introduced by Gupta et al. in 2008 [17]. As Fig. 1.4 shows, it is a wearable platform-type robot that covers the forearm and wrist motions. Several control strategies including PD (proportional derivative) position control, force control, and impedance control are implemented for controlling the robot [17].

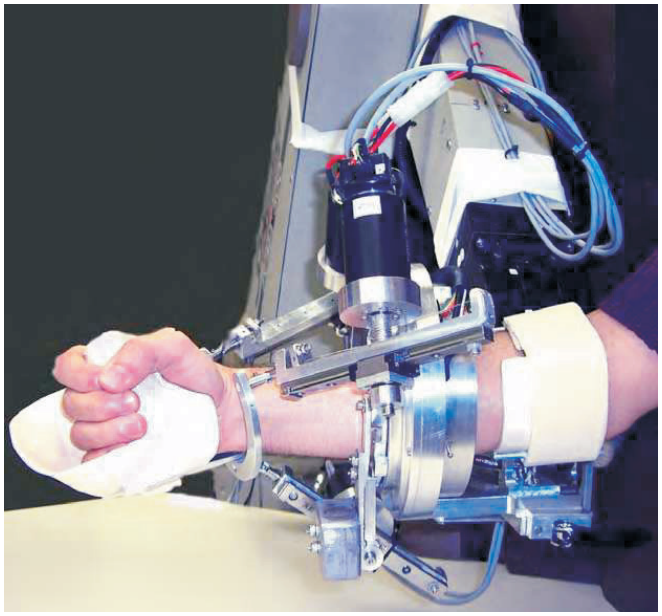

Figure 1.4: RiceWrist rehabilitation robot developed by Gupta et al. [17].

A robot called UHD (universal haptic drive) was designed and developed for the rehabilitation of the arm, forearm, and wrist by Oblak et al. in 2009 [18]. The robot has two modes which in the first mode it has 1 DoF and just covers one motion of the arm and in the second mode, it has 2 DoF and covers forearm motion and one of the wrist motions. Depending on how the grasping handle of the robot is installed, it can switch between two motions of the wrist. The robot is equipped with 2 DC (direct current) motors which pull cables connected to a rod that has a spherical joint at the base. Two springs are used as SEA (series elastic actuator) on cables for controlling the stiffness of the robot by implementing impedance control. It has a force sensor on the rod for measuring the interaction force between the patient's hand and the robot. The robot was tested on a stroke patient in a clinical trial for 6 sessions and some improvements were observed after these therapies [18]. A 3 DoF exoskeleton robot was designed by Masia et al. in 2009 which covers movements of the wrist and forearm [19]. In 2013 it was upgraded and developed by Squeri et al. and an impedance control

strategy was used for controlling the robot [20]. The robot was tested on 9 patients in 10 sessions and notable improvements were observed in their active range of motions [20]. An exoskeleton robot named IntelliArm which aims the upper limb rehabilitation was developed by Ren et al. in 2012 [21]. The robot has 6 DoF which 4 of them are active, which means driven by actuators, and the others are passive. The four active DoF cover the motions of the shoulder, elbow, forearm, and flexion/extension of the wrist. There is a DC motor for controlling each of the active joints. Position control is used for the passive mode of the robot and impedance control was implemented for the active mode of the robot. The robot was tested on 3 stroke patients in a clinical trial and notable improvements were observed in their ROM (Range of Motion) [21]. In 2013 a 3 DoF robot called Wrist Gimbal was introduced by Martinez et al. [22]. As Fig. 1.5 shows, it was specially designed for the wrist and forearm and is able to perform several control strategies including position control for passive mode in which the patient moves the robot without exerting any force and is useful for ROM measurement and resistive mode in which the patient tries to overcome the robot exerting force [22].

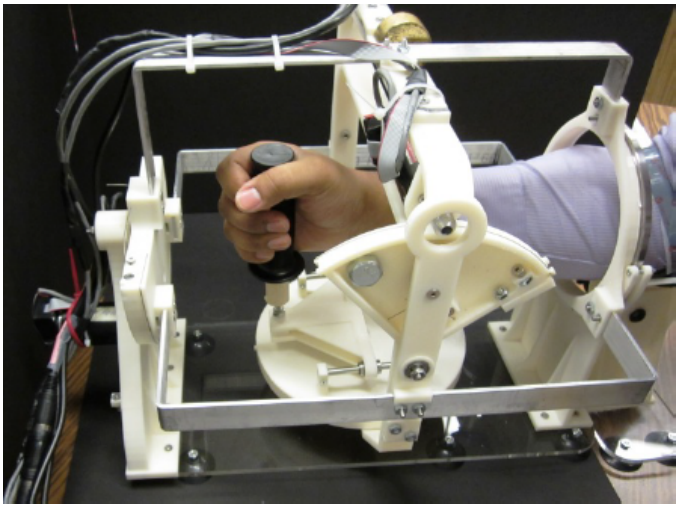

Figure 1.5: Wrist Gimbal rehabilitation robot developed by Martinez et al. [22].

A 3 DoF wrist and forearm rehabilitation robot was introduced by Atlihan et al. in 2014 [23]. As Fig. 1.6 shows, the robot structure is serial and is equipped with a force sensor and has the ability to switch between position control and force control [23]. In 2018 the robot was tested on healthy people as well as patients in a clinical trial and upper limb performance improved after therapy [24].

Figure 1.6: Wrist and forearm rehabilitation robot developed by Akdogan et al. [24].

In 2014 a cable robot named CDWRR was developed for rehabilitation of the forearm and wrist by Cui et al. [25]. The robot is a wearable exoskeleton that has a parallel structure with 3 DoF [25]. The robot has a handle that is suspended from 4 cables and each cable tension is controlled by a separate servomotor with shortening and lengthening of the cable. The robot is able to cover the wrist and forearm motions [26]. It uses a torque-field controller which provides the required force to help the patient to perform the defined task trajectory [26]. A single DoF robot named CR2-Haptic was introduced and developed by Khor et al. in 2014 [27]. As Fig. 1.7 shows, it is able to cover all degrees of freedom of the wrist and the forearm separately but not simultaneously. To reach this purpose different types of grasping handles are designed and also the robot is needed to be installed in different positions to cover each of the wrist and the forearm DoF [27]. It was tested on 7 patients in a clinical trial in 30 sessions and a considerable improvement was observed [28].

Figure 1.7: CR2-Haptic rehabilitation robot developed by Khor et al. [27].

In 2014 a rehabilitation robot for the wrist and fingers was developed by Amirabdollahian et al.

[29]. It is a wearable exoskeleton robot that covers the flexion/extension of the wrist and fingers flexion. The robot was tested on 23 stroke patients in their homes for checking its performance [29]. In 2015 a soft robot was introduced and developed by Bartlett et al. for the rehabilitation of the forearm and wrist [30]. It is a wearable soft robot actuated by pneumatic muscles and an air pump and it has the capability to cover 3 DoF of the forearm and wrist. It was tested on a healthy person for observing and evaluating the performance of the robot [30]. A wearable rehabilitation robot named ETS-MARSE was developed by Rahman et al. in 2015 [31]. As Fig. 1.8 shows, the robot is an exoskeleton with 7 DoF which aims motions of the shoulder, elbow, forearm, and wrist. It is equipped with 7 Dc motors, harmonic drives, potentiometers, and force sensors. It was tested on four healthy subjects to evaluate the robot's performance [31].

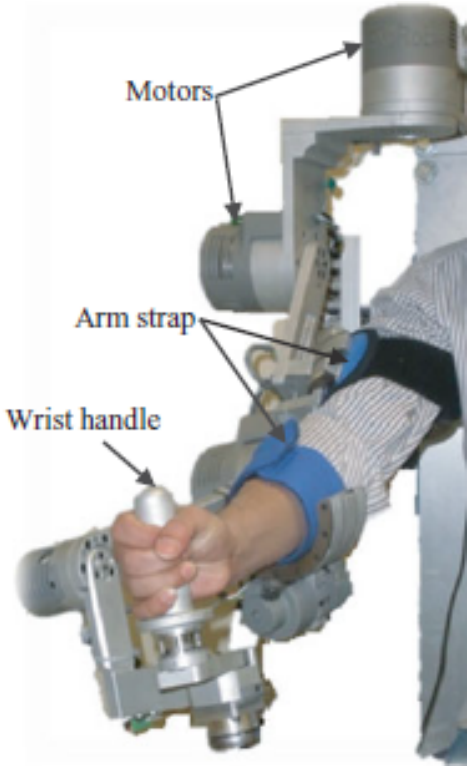

Figure 1.8: ETS-MARSE rehabilitation robot developed by Rahman et al. [31].

Another wrist and forearm rehabilitation robot named NU-Wrist was introduced by Omarkulov et al. in 2016 [32]. As shown in Fig. 1.9, the robot is a 3 DoF exoskeleton with a serial structure and has the ability to do passive therapy. The initial 3D printed model was tested on healthy subjects [32]. A 2 DoF wearable robot for the rehabilitation of the elbow and wrist was developed by Beom

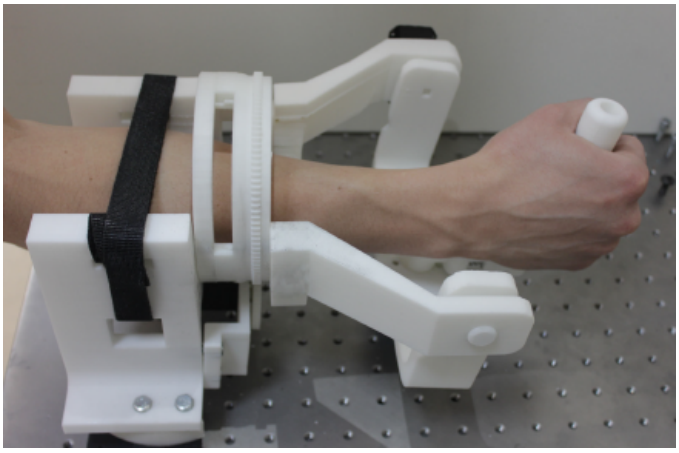

Figure 1.9: NU-Wrist rehabilitation robot developed by Omarkulov et al. [32].

et al. in 2016 which just covers the flexion-extension of the wrist [33]. It is equipped with a Dc motor and a torque sensor for each of the joints. It was tested for the rehabilitation of 20 patients in a clinical trial [34].

A 2 DoF wearable rehabilitation robot was introduced and developed by Higuma et al. in 2017 [35]. As shown in Fig. 1.10, it is able to cover the flexion/extension and radial/ulnar deviation motions of the wrist. It has two linear actuators connected to two blade springs. If the actuators go forward or backward together, the robot does the flexion/extension movement and if one of them goes forward and the other one goes backward, the robot does the radial/ulnar deviation movement [35]. The robot ROM was measured using a camera and a force sensor was used for checking the robot force. A simple prosthetic hand and forearm model with a universal joint as the wrist joint was designed for testing and evaluating the robot's capabilities [35].

In 2018 a wrist rehabilitation robot named WReD with only one DoF was introduced by Xu et al. [36]. As shown in Fig. 1.11, it is equipped with a DC motor gearbox, torque sensor, encoder, and an adjustable handle for interaction with the human hand. Depend on how the handle is installed, every time it can cover one of the wrist degrees of freedom [36]. It uses an impedance control strategy, a double loop control scheme with a PID (proportional integral derivative) position controller in the inner loop, and a force controller in the outer loop to guarantee position trajectory tracking and safe interaction simultaneously. For checking the performance it was tested on a healthy subject [37].

A 3 DoF wrist and forearm rehabilitation robot named WRES was introduced and developed by

Figure 1.10: Rehabilitation robot developed by Higuma et al. [35].

Figure 1.11: WReD rehabilitation robot developed by Xu et al. [37].

Buongiorno et al. in 2018 [38]. As shown in Fig. 1.12, it has 3 brushless DC motors, one force sensor, and a cable-driven capstan mechanism designed for wrist motions. It was tested on a healthy subject for checking out the performance of the robot [38].

In 2020 a parallel robot named PWRR was introduced by Zhang et al. [39]. As shown in Fig. 1.13, the robot is pneumatically actuated and has 2 DoF for covering the wrist motions. An air compressor is used for pressurizing the two pneumatic actuators and a magnetic sensor is used for each of them to measure the position of the piston inside the cylinder as feedback. The air volume and pressure behind the piston are controlled using pneumatic valves. The robot is able to perform

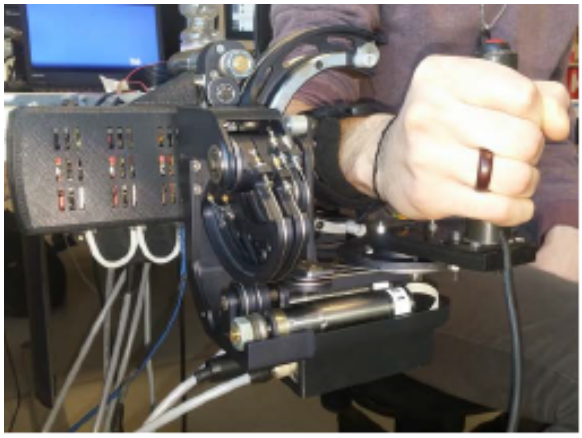

Figure 1.12: WRES rehabilitation robot developed by Buongiorno et al. [38].

passive rehabilitation therapy using a position control strategy [39].

Figure 1.13: PWRR rehabilitation robot developed by Zhang et al. [39].

In this thesis, a 2 DoF compact size, portable rehabilitation robot with a newly designed structure for the wrist is introduced. The proposed design has a remote center of motion and can rotate the wrist about its center of rotation. Based on the wrist rehabilitation requirement we first proposed the kinematic architecture to cover the required motion as well as having a suitable kinematic performance. based on the proposed kinematic the mechanical design of the robot is completed and a prototype is developed. The control of the robot is based on the position control with a limit on the torque of the motors to keep the interaction force with the wrist in the allowable range.

1.1 Problem Definition

After-stroke patients face a kind of disability in one side of their bodies. They need rehabilitation therapy done by a physiotherapist to regain their ability to move their upper and lower limbs. Rehabilitation therapy is a long time, repetitive, and expensive process. Using rehabilitation robots can have many benefits for the patients and the health care system. There are different types of rehabilitation robots, each one focusing on different parts of the upper limb. Some of the existing rehabilitation robots focusing on the human wrist are bulky, with the actuators installed on the moving links. They are also risky as the human hand goes inside their structure. Some other robots can not provide both degrees of freedom of the human wrist simultaneously, and some robots suffer deficiency in the actuation system. This thesis aims to develop a portable, low-cost, and lightweight wrist rehabilitation robot for home use which is safe as the human's hand lies out of the robot's structure. We also introduce a new approach for designing safe trajectories for controlling the robot to avoid excessive torques on the patient's wrist.

1.2 Research Objectives

- To design and develop a 2-DoF wrist rehabilitation robot which is portable, lightweight, low-cost, and convenient for home use.
- To design safe optimal trajectories for controlling the wrist rehabilitation robot using dynamical model of the human wrist and the constraints over the maximum allowable torques and range of motions.

1.3 Thesis Contributions

- Optimal Design and development of a low-cost, 3D printed wrist rehabilitation robot.
- Employing a remote center of motion mechanism for wrist rehabilitation application.
- Design of a novel actuation system, enabling the actuators to be grounded.

- Designing optimal safe trajectories in terms of applied torque on the patient's hand, considering the constraints over the maximum allowable torques and range of motions of the hand.

1.4 Thesis Layout

This thesis consists of the following chapters:

- **Chapter 1:** This chapter presents the introduction, literature review, current existing designs and their characteristics.

- **Chapter 2:** presents a portable 3D printed wrist rehabilitation robot with a novel actuation system. The kinematic design of the robot, including the linkages architecture, actuation mechanism, and end-effector design, is explained. The kinematic modeling of the robot and the optimal design are described, and then this kinematic model is validated. The development of the robot will be demonstrated, and at last, the experimental results will be shown by giving several trajectories to the robot. This chapter is based on a journal paper which is under review.

- **Chapter 3:** presents a novel approach for designing an optimal trajectory for controlling our wrist rehabilitation robot based on the dynamical model of the human wrist. The optimal trajectory is designed with constraint in the torque generated in the human wrist to guarantee that the interaction between the human wrist and the robot is safe. This chapter is based on a paper which is in progress for submission.

- **Chapter 4:** demonstrates the drawings of the whole structure of the robot with the detailed views and the designed parts. Also, the fabrication process and experimental setup are explained. Finally, the test procedure on a healthy person is described.

- **Chapter 5:** This chapter describes the conclusion and proposes several works that can be done in the future to improve the robot.

Chapter 2

A Portable Low-cost 3D Printed Wrist Rehabilitation Robot: Design and Development

This article proposes a two-degrees-of-freedom robot for wrist rehabilitation, referred to as MOCH (Persian equivalent name for wrist). The MOCH mechanism comprises a remote center of motion (RCM) mechanism with a rotation center outside of the robot structure. When the patient holds the robot end-effector, coinciding the RCM of the robot with the rotation axis of the wrist, allows pure rotational motion of the hand. As the rotation point lies out of the robot structure, there is less risk of interference between the patient and the robot. Furthermore, MOCH benefits a novel actuation that enables the actuators to be grounded, reducing the inertia and the size of the robot and eliminating difficulties with feeding power to actuators on moving linkages. The optimal design of MOCH is provided considering the mechanical criteria and requirements of the wrist rehabilitation robot. Based on the proposed design, a prototype of the robot is developed with a mass of 1.3 kg using 3D printing method. To validate the efficacy of MOCH in practice, a trajectory tracking control strategy is implemented for passive wrist rehabilitation.

2.1 Introduction

Upper limb impairment is a typical result of stroke, and a majority of patients have to experience a long time of motor impairment. Based on the brain's neuroplasticity, part of the motor skill can be restored by receiving rehabilitation training. However, the rehabilitation procedure is time-consuming and demands experienced therapists. Rehabilitation robots can overcome these limitations by removing the shortage of experienced therapists in remote areas and can operate for more extended periods. One of the first and most noteworthy robots developed for upper limb rehabilitation is MIT-MANUS which has five DoF [5]. The primary version of MANUS had two DoF introduced in [6], which is a planar SCARA mechanism with one DoF for the shoulder and one DoF for the elbow. A new version of MANUS was introduced in [6] by adding three DoF modules to cover wrist and forearm motion. Bi-Manu-Track is another rehabilitation device with two DoF especially developed for the forearm and wrist by Hesse et al. [14]. It covers one DoF for the wrist, and the other one is reserved for the forearm. A robot called Universal Haptic Drive (UHD) was developed for the rehabilitation of the arm, forearm, and wrist by Oblak et al. [18]. Masia et al. [19] designed a three DoF exoskeleton robot that covers movements of the wrist and forearm. This design was improved and developed by Squeri et al. [20] by integrating an impedance controller. Martinez et al. [22] introduced a three DoF robot called Wrist Gimbal. It was specially designed for the wrist and forearm and can execute multiple control strategies, including position control and force control modes [22]. A three DoF wrist and forearm rehabilitation robot was introduced by Atlihan et al. [23] which has a serial kinematic structure and is equipped with a force sensor and can switch between position control and force control modes. Cui et al. [25] introduced another robot named CDWRR to rehabilitate the forearm and wrist. CDWRR is a wearable exoskeleton that has a parallel structure with three DoF. Its handle is suspended from four cables, and a separate servomotor controls each cable tension with shortening and lengthening of the cables [26]. Khor et al. [27] developed a single DoF robot named CR2-Haptic that covers all degrees of freedom of the wrist and the forearm separately via different types of grasping handles. Amirabdollahian et al. [29] developed a wearable exoskeleton robot for the wrist and fingers that cover the flexion/extension of the wrist and fingers flexion. Another wrist and forearm rehabilitation robot named NU-Wrist was

introduced by Omarkulov et al. [32]. The robot is a three DoF exoskeleton with a serial kinematic structure and can do passive therapy. The initial 3D printed model was tested on healthy participants [32]. A wrist rehabilitation robot named WReD with only one DoF was introduced by Xu et al. [36]. It is equipped with a torque sensor, encoder, and an adjustable handle to be held by hand. Depending on the configuration of the handle, in each case, it can cover one of the wrist DoF [36]. A three DoF wrist and forearm rehabilitation robot named WRES was introduced and developed by Buongiorno et al. [38]. It has three brushless DC motors, one force sensor, and a cable-driven capstan mechanism designed for wrist motions. It was tested on a healthy subject for checking out the performance of the robot [38]. A parallel robot named PWRR was introduced by Zhang et al. [39]. The robot is pneumatically actuated and has two DoF for covering the wrist motions. An air compressor is used to pressurize the two pneumatic actuators and a magnetic sensor for the position measurement. The air volume and pressure behind the piston are controlled using pneumatic valves. The robot is able to perform passive rehabilitation therapy using a position control strategy.

What was discussed above was a summary of the available wrist rehabilitation robots in the literature. Most of the proposed designs for wrist rehabilitation are bulky with a serial kinematic structure similar to MIT-MANUS, such as the robots developed by Squeri et al. [20], WRES [38], Wrist Gimbal [22], and the robot [23] developed by Atlihan et al. The weakness of these designs is that the actuators are mounted on a rotating arm, and the structure could be risky to the patient as the patient hand lies within the robot's structure. In several existing designs such as CR2-Haptic [27], Bi-Manu-Track [14], and WReD [36] the robot cannot provide both of the required DoF for wrist rehabilitation simultaneously; the whole structure of the robot needs to be reconfigured, which is not convenient for the user. Some other designs suffer deficiency in the actuation system requiring pneumatic actuation like PWRR [39] and a soft robot developed by Bartlett et al. [30]. The other designs, such as RiceWrist [17], and CDWRR [25] have complicated kinematic chains with bulky structures, and the patient hands lie within the structure of the robot. Considering the shortcoming of the mentioned existing designs, we propose a novel two DoF wrist rehabilitation robot called MOCH. To design MOCH our objectives are the safety of the patient, simplicity of the design and manufacturing process, portability, and low cost of production. The proposed design is based on the parallelogram-based remote center of motion (RCM) mechanism. Although there

are various types of RCM mechanism in the literature such as [40, 41, 42, 43], the ones based on the parallelogram mechanism have the advantage of being simple for analysis and manufacturing. In the RCM mechanism, the end-effector has a center of rotation outside of the robot structure. This allows the rotation of the wrist in a fixed point outside of the robot structure, minimizing the risk of interference. Based on the wrist rehabilitation design requirements, we first design a kinematic architecture to cover the required motion. Secondly, a novel actuation of the mechanism is introduced to locate the actuators at the robot's base. Then we discuss the design of the end-effector by transforming the shape of the linkages. Considering the cost-effective manufacturing process and simple design, the robot's mechanical design is provided to be manufactured with simple elements via 3D printing method. The validity of the proposed design regarding the design requirements and motion characteristics is verified through a working prototype of the robot. Finally, the robot is analyzed for passive wrist rehabilitation practice with a periodic trajectory.

The remaining structure of this chapter is as follows; in Section 2.2, we present the kinematics and the dynamics of the human wrist. In Section 2.3, considering the design criteria, we discuss on the suitable mechanism and its architecture, a novel actuation design, as well as the design of the robot end-effector. The kinematic analysis and the optimal design of the robot considering the kinematic constraints and performance indices are then disclosed in Section 2.4. Kinematic validation is done in Section 2.5. In Section 2.6, we overview the implemented setup. Finally, in Section 2.7 the performance of the robot is investigated in a passive exercise while giving a predefined trajectory to the robot.

2.2 Kinematics and Dynamics of the Wrist Motion

The human wrist has two types of rotational motions; referred to as flexion/extension and radial/ulnar. As shown in Fig. 2.1, flexion/extension is the up and down motion of the wrist while the radial/ulnar is the sideway motion. The range of motion of the human wrist DoF is not symmetric. The maximum allowable range of motion (ROM) for the up and down motion of the wrist is from 54° in flexion to 60° in extension [44]. Moreover, for the sideway motion, the maximum ROM is from 17° in radial to 40° in ulnar [44]. However, 70% of the daily activities lie in the 42% of ROM,

referred to as activities of daily living ROM (ADLs ROM) [45].

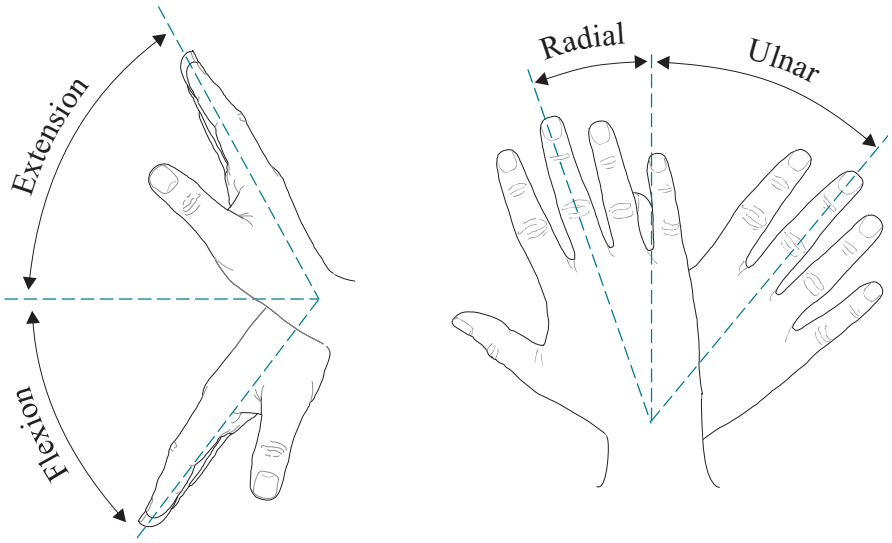

Figure 2.1: Wrist motions and degrees of freedom.

Table 2.1: Wrist ADLs ROM

Motion type	ADLs ROM
Flexion/Extension	$-54°$ to $60°$
Radial/Ulnar	$-17°$ to $40°$

Considering the wrist as a universal joint, the governing dynamic model of the wrist rotation can be expressed as the following equation [46]. In the equation, θ and ϕ show the rotations around the wrist center of rotation for the flexion-extension and radial-ulnar directions, respectively. τ_θ and τ_ϕ are the torques generated in the wrist for θ and ϕ directions, respectively. Also, m is the mass of the hand, and r is the distance between the center of the mass of the hand and the wrist center of rotation.

$$\begin{bmatrix} \tau_\theta \\ \tau_\phi \end{bmatrix} = \begin{bmatrix} I_\theta & 0 \\ 0 & I_\phi \end{bmatrix} \begin{bmatrix} \ddot{\theta} \\ \ddot{\phi} \end{bmatrix} + \begin{bmatrix} C_\theta & C_{\theta\phi} \\ C_{\theta\phi} & C_\phi \end{bmatrix} \begin{bmatrix} \dot{\theta} \\ \dot{\phi} \end{bmatrix} + \begin{bmatrix} K_\theta & K_{\theta\phi} \\ K_{\theta\phi} & K_\phi \end{bmatrix} \begin{bmatrix} \theta \\ \phi \end{bmatrix} + \begin{bmatrix} mgr\cos\theta \\ 0 \end{bmatrix} \quad (1)$$

in which the inertia (I) and gravity matrices parameters of the equation are average values for 6 healthy persons aged between 19 to 28 years old measured in [46] and stiffness matrix (K) parameters are the average values for 15 healthy persons aged between 20 to 27 years old measured in [45]. Also according to [46] the damping matrix (C) is 5 percentage of stiffness matrix. These parameters are summarized in Table 2.2.

Table 2.2: Dynamic parameters of the wrist.

Inertia (kgm^2)	Stiffness (Nm/rad)	Damping (Nm/rad^2)	Gravity effect (N.m)
$\begin{bmatrix} 0.0022 & 0 \\ 0 & 0.0022 \end{bmatrix}$	$\begin{bmatrix} 0.85 & -0.27 \\ -0.27 & 2.02 \end{bmatrix}$	$\begin{bmatrix} 0.043 & -0.014 \\ -0.014 & 0.101 \end{bmatrix}$	$\begin{bmatrix} 0.218 \\ 0 \end{bmatrix}$

2.3 Kinematic Design of the Robot

There exist two main types of wrist rehabilitation robots, robotic exoskeletons, and end-effector-based robots. In this article, our focus is on the latter one, in which the patient holds the end-effector of the robot, and the wrist moves with the robot in a prescribed trajectory. The first design objective is on the kinematics, which requires covering two pure rotations of the wrist. For the second objective, we take into account the patient's safety and minimum risk of interference of the hand with the robot. The other objective in the development of MOCH was a cost-effective design to be affordable for low-income patients. It requires a simple design of the mechanical parts, an inexpensive and accessible manufacturing process. Moreover, a compact and portable design suitable for home usage should be met by the proposed design. Considering the requirement for two pure rotational DoF and the risk of interference with the patient, we chose a category of the mechanisms referred to as the remote center of motion (RCM) mechanism. An RCM mechanism has a remote center of rotation that lies out of the robot structure and can rotate the hand without having any risk of interference [47]. The RCM mechanisms are well known in the surgical robotic field. However, to the best knowledge of the authors, these types of mechanisms have not been explored for wrist rehabilitation applications yet. In this study, we propose a double parallelogram

RCM mechanism with a novel actuation system for MOCH. The novel actuation of the mechanism allows the actuators to be positioned at the base of the robot, decreasing the inertia of the moving parts and the size of the robot while increasing the reliability. We also propose a new design for the distal linkages (end-effector) of the mechanism to be held by the patient during rehabilitation practice. The dimension of these distal linkages and their connection is chosen in a way to position the center of rotation of the wrist at the RCM of the mechanism.

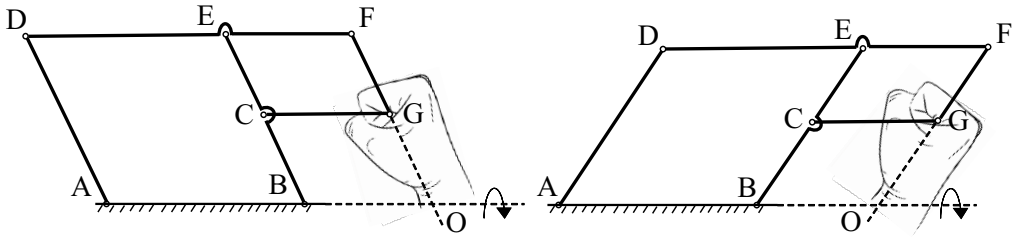

Figure 2.2: Parallelogram-based RCM mechanism with the RCM point (O) coinciding with the rotation axis of the wrist.

Referring to Fig.2.2, the parallelogram mechanism in its simplest design has five linkages, with AB being the ground of the mechanism. The motion of the parallelogram mechanism allows link FG to have a pure rotation about O, which lies out of the robot structure. When a user holds FG such that the center of wrist rotation coincides with the RCM point, the mechanism can provide the flexion/extension motion of the wrist. The radial/ulnar motion is also provided through the out-of-plane rotation of the ground, along an axis passing through AB. In what follows, we discuss the mechanical design of the robot kinematic architecture and its component considering the design criteria. Considering the parallelogram mechanism as our candidate, a prototype of MOCH is developed as depicted in Fig.2.3. The mechanism is installed vertically to be used by the patient sitting on a desk. This architecture is comprised of a novel actuation mechanism powered by a lead screw, a rotating arm, a parallelogram mechanism mounted on the rotating arm, and the end-effector.

2.3.1 Linkages Architecture

In the proposed design, the motion of the parallelogram mechanism is provided using an extra linkage mounted on a linear guide and coupled to a lead screw. The connection of the coupling linkage with the parallelogram mechanism can be provided with different configurations as depicted in

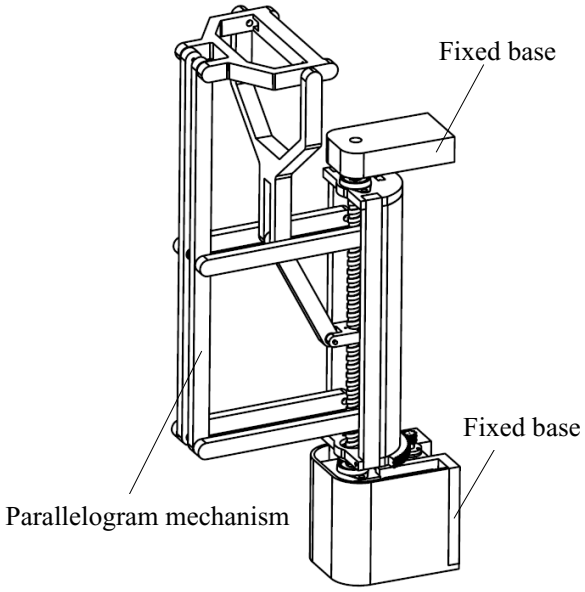

Figure 2.3: CAD model of MOCH.

Fig.2.4. As there are five moving linkages in the mechanism, there would be five different configurations for the connection of the coupling linkage.

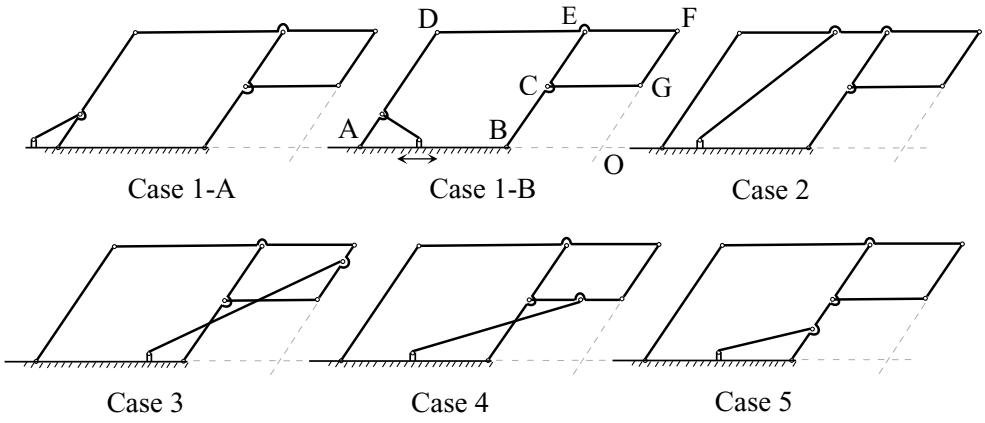

Figure 2.4: Possible configuration of connecting the coupling link to the RCM mechanism.

Based on the design criteria, the third and fourth possible architecture are not suitable as both cases pass BCG, which has a risk of collision with the patient hand. In case-2, we need to have a large coupling link which also requires an additional joint on DE. Moreover, in the first possible configuration, case 1-A is not suitable as the whole stroke of the coupling link is outside of the AB, which leads to a bulky structure. Thus the feasible solutions are case 5 and case 1-B. Comparing

these two feasible solutions, case 5 has the benefit of being easily coupled to the parallelogram mechanism at point C without adding extra joints to the mechanism. However, for case 1-B, an extra joint should be added to the mechanism.

2.3.2 Actuation Mechanism

Generally, in the parallelogram-based RCM mechanism, the parallelogram mechanism is mounted on a rotating arm. Also, its actuator is mounted on the rotating arm. This leads to higher inertia of the moving parts, which requires more powerful actuators than the design where the actuators are on the ground. The other shortcoming of such a structure is the wiring system issues on the rotating mechanism, which might be risky. Moreover, in this design, the moving parts are bulky. To overcome the existing problem in such structures, we introduce a novel actuation system for MOCH where both of the actuators are grounded, as shown in Fig.2.5.

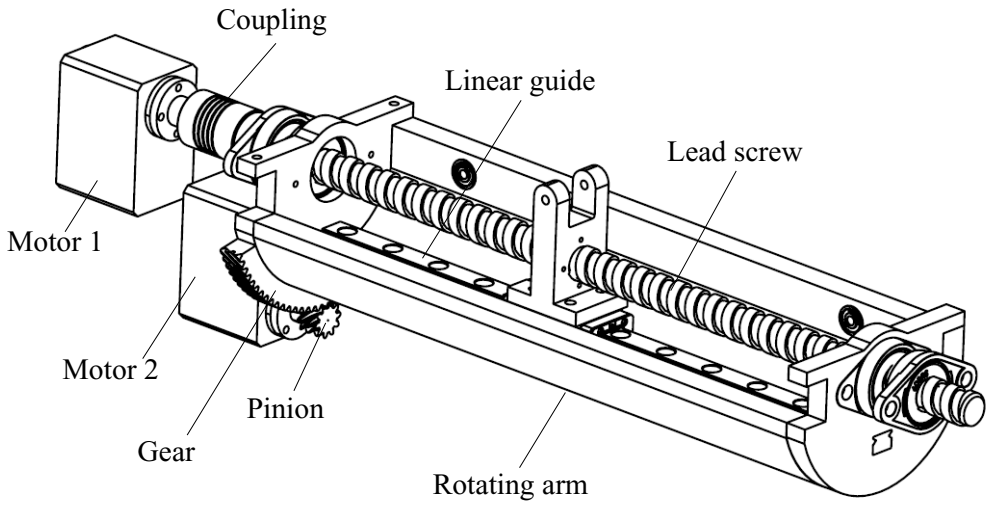

Figure 2.5: The novel actuation of MOCH.

As shown in Fig.2.5, the proposed actuation system is comprised of a rotating arm, with the axis of rotation being the same as the axis of the lead screw. The linear motion is provided with the coupling of the lead screw nut to a linear guide. Additionally, the motion of the base is provided via a pinion coupled to a gear on the rotating arm. This actuation system leads to the coupling of the inputs, which will be discussed in detail in the kinematic modeling. For better clarification, consider

the lead screw to be fixed while the base of the parallelogram is rotating. As the lead screw nut is coupled to the mechanism, it will have the same rotation as the rotating arm. On the other hand, as the nut is mounted on the lead screw, any rotation of the nut will result also in a linear movement. Thus the rotation of the robot for radial/ulnar motion also leads to a flexion/extension motion, which can be simply compensated with the knowledge of the robot kinematics. For the cheap cost of manufacturing, and considering the availability of the mechanical components anywhere, we have chosen 3D printers lead screw for the actuation system which is in the market in standard sizes.

2.3.3 Rotating Arm

The rotating arm of the mechanism supports the parallelogram linkage and is coupled to a pinion with a gear mounted on it. It is to be noted that in this prototype, this gear is 3D printed; however, it may be replaced with a capstan drive or any suitable power transmission system. The lead screw works as the rotation axis of the rotating arm. The rotating arm is mounted on the lead screw using two bearings at the ends. Additionally, a linear guide is integrated at the bottom of the rotating arm, and its carriage with the length of $4cm$ is fixed to the nut of the lead screw.

2.3.4 End-Effector

The RCM mechanism can rotate the payload about a fixed point out of the robot structure. To make use of this architecture for the wrist rehabilitation purpose, the end-effector should be designed to be held with the patient while the axis of the rotation of the wrist coincides with the RCM of the mechanism. To have a compact design and minimizing the mechanical parts, we have transformed the linkages of the mechanism to be used as the end-effector, as depicted in Fig.2.6. As it is clear from the figure, the transformed linkages are fork-shaped and hinged to each other at one end via revolute joints and at the other end are jointed to the linkage of the mechanism. For link FG of the mechanism, which is the end-effector, we have also considered a bar to be held by the patient.

Considering the proposed design for the end-effector, the length of the linkage BC is obtained based on the distance of the end-effector and the wrist rotation axis. Additionally, for the length of FG, there should be enough space for the hand when holding the end-effector and its coupling with link EF.

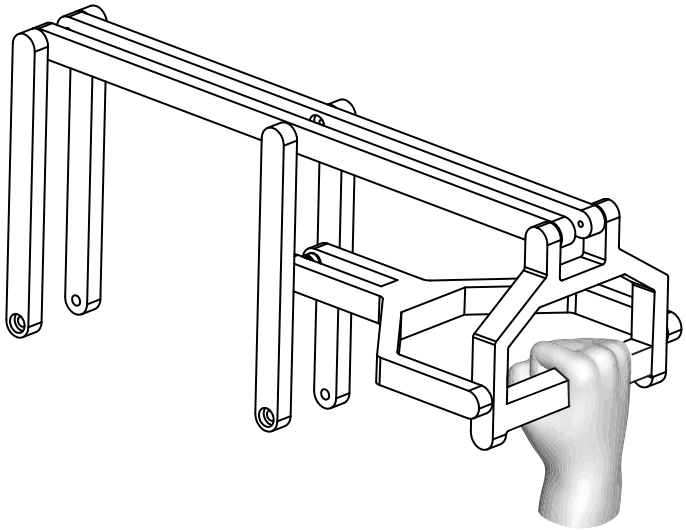

Figure 2.6: The robot end-effector design to be held by the patient

2.4 Kinematic Modeling of the Robot

MOCH is designed for passive wrist rehabilitation, where a predefined trajectory for the flexion/extension and radial/ulnar motion is given to the patient wrist. Such maneuver requires the knowledge of the robot kinematics to map the actuator motion to that of the robot end-effector. Additionally, we require the kinematic modeling for the optimal length of the remaining linkage of the mechanism in this section, namely a and l as shown in Fig. 2.7. The kinematic structure of the robot consists of two parallelogram mechanisms coupled to each other that allow the pure rotation of the end-effector FG about a remote center O. The parallelogram mechanism is mounted on a rotating arm at points A and B via revolute joints. The rotating arm is also hinged to the ground via revolute joints, with AB being the axis of rotation. Thus, the configuration of the end-effector can be represented via two pure rotations θ and ϕ about point O.

In the proposed design, the motion of the parallelogram mechanism is provided with a slider coupled to the lead screw via a nut. The lead screw also works as the rotation axis of the rotating arm. With the base rotation, the nut, which is also a part of the parallelogram mechanism will have the same rotation. As the nut is constrained to the lead screw, it also moves along the lead screw axis. Thus, the parallelogram mechanism will move with the motion of the rotating arm. This leads to the coupling motion of θ, which is to be considered in the kinematic modeling. Such an actuation

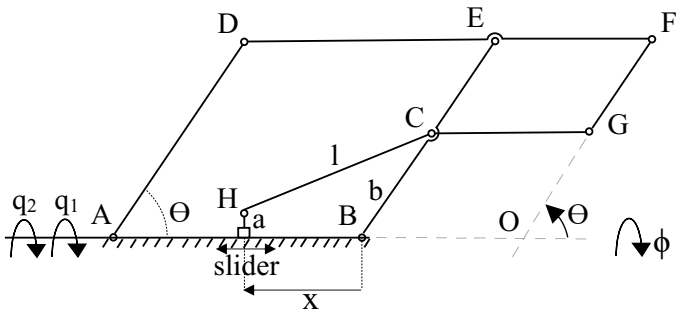

Figure 2.7: Schematic representation of the mechanism: q_1 and q_2 are the inputs for the ball screw and rotating arm, respectively, and θ and ϕ are the outputs.

system allows us to position the actuators at a fixed base, which is one of the contributions of our proposed mechanism, as mentioned throughout the chapter. Representing the joint space variables by q_1 and q_2, the inverse kinematic of the robot is given by:

$$\begin{cases} q_1 = \frac{x}{k_1} + \phi \\ q_2 = \frac{1}{k_2}\phi \end{cases} \tag{2}$$

in which k_1 and k_2 are the gear ratio of the lead screw, and the rotating arm gear, respectively. The value of x, measured from B in equation (2) can also be found through the following equation:

$$x = -bcos(\theta) + \sqrt{l^2 - (bsin(\theta) - a)^2} \tag{3}$$

where the length l and b, can be found in Fig. 2.7. The second step after obtaining the kinematic model is the Jacobian modeling. The Jacobian matrix determines the velocity relation between joint space variables and that of the workspace. Additionally, the kinematic performance and singularity analysis of the mechanism requires the Jacobian matrix. In parallel robots, the Jacobian matrix is defined as the following equation where $\boldsymbol{q}$ is the joint variables vector and $\boldsymbol{X}$ is the workspace variables vector.

$$\dot{\boldsymbol{q}} = \boldsymbol{J}\dot{\boldsymbol{X}} \tag{4}$$

To find the Jacobian, equation (3) is differentiated with respect to time,

$$\dot{x} = b\dot{\theta}sin(\theta) - \frac{bcos(\theta)(bsin(\theta) - a)}{\sqrt{l^2 - (bsin(\theta) - a)^2}}\dot{\theta} = \eta\dot{\theta} \tag{5}$$

Thus the Jacobian matrix is

$$\begin{bmatrix} \dot{q_1} \\ \dot{q_2} \end{bmatrix} = \begin{bmatrix} \frac{\eta}{k_1} & 1 \\ 0 & \frac{1}{k_2} \end{bmatrix} \begin{bmatrix} \dot{\theta} \\ \dot{\phi} \end{bmatrix} \tag{6}$$

Referring to equation (6) the singularity of the mechanism occurs when $\eta = 0$ resulting:

$$sin(\theta) = \frac{a}{b \pm l} \tag{7}$$

which occurs when CH and BC are colinear. As discussed earlier, the length of $BC = b$ was selected based on the size of the hand and, AB was chosen based on the standard size of lead screws in the market. Thus the remaining lengths of the linkages are a and l. In what follows we obtain an optimal candidate for l and a based on the kinematic constraints and performance indices.

First of all, for the compact design, the slider should lie within the allowable range of stroke for the lead screw within the required workspace for flexion/extension motion. This can be defined as the following constraint:

$$\begin{cases} x_{\theta_{min}} > \delta \\ x_{\theta_{max}} < d - \delta \end{cases} \tag{8}$$

in which $\theta_{min} = 30^\circ$ corresponds to the maximum of the extension range of the hand and $\theta_{max} = 144^\circ$ corresponds to the maximum of the flexion range. It is to be noted that $\theta = 90^\circ$ while the hand is in its neutral position. Substituting (3) in (8) results:

$$\begin{cases} -bcos(\theta_{min}) + \sqrt{l^2 - (bsin(\theta_{min}) - a)^2} > \delta \\ -bcos(\theta_{max}) + \sqrt{l^2 - (bsin(\theta_{max}) - a)^2} < d - \delta \end{cases} \tag{9}$$

in which δ is the half length of the linear carriage. Moreover, d is the total length of the allowable lead screw stroke within the rotating arm considering the clearance of the carriage at the two ends of the stroke. The suitable region for the selection of l and a using Eq.(9) is specified with two black curves in Fig.2.8. Additionally, there are extra constraints for the existence of the triangle BCH in

θ_{min} and θ_{max}. Defining $m = \sqrt{a^2 + x^2}$ the inequality of the triangle existence can be defined as:

$$\begin{cases} m_{\theta_{min}} + l > b \\ m_{\theta_{min}} + b > l \\ l + b > m_{\theta_{min}} \end{cases} , \begin{cases} m_{\theta_{max}} + l > b \\ m_{\theta_{max}} + b > l \\ l + b > m_{\theta_{max}} \end{cases} \tag{10}$$

Moreover, we should also check that the required trajectory for the flexion/extension does not pass the singularity of the mechanism which should meet the following equations:

$$\begin{cases} sin\theta_{min} > \frac{a}{b-l} \\ sin\theta_{max} > \frac{a}{b+l} \end{cases} \tag{11}$$

Using Eq.(9), as it is shown in Fig.2.8, it is apparent that $l > 0.085$(m) which is greater than $b = 0.075$(m), thus $b - l$ in Eq.(11) is negative. Being so, the suitable region considering the constraint Eq.11 lies within two lines, depicted via white color in Fig.2.8. The discussed constraint of the problem gives us a common region for the suitable selection of l and a. To find one optimum solution within this region, we use the Jacobian condition number (κ) which is a measure of kinematic isotropy, defined as:

$$\kappa = \sqrt{(\lambda_{max}/\lambda_{min})} \tag{12}$$

In which λ_{min} and λ_{max} are the eigen values of JJ^T and $\frac{1}{\kappa}$ is always between 0 and 1. It is desirable to have $\frac{1}{\kappa}$ as much closer to 1 for better dexterity. It is to be noted that the condition number is a local indication for the dexterity of a robot. To evaluate the dexterity of the robot over a given workspace, we use the global conditioning index (GCI) introduced by Gosselin [48] as:

$$GCI = \frac{\int_W \frac{1}{\kappa}.dW}{\int_W .dW} \tag{13}$$

which corresponds to the average value of $\frac{1}{\kappa}$ within the robot workspace. The value of GCI for different ranges for a and l is depicted in Fig.2.8. This figure also shows the regions that meet the constraint of the problem. The region between the black curves is defined by Eq.9 and white lines

define the suitable region to meet Eq.11. The triangular existence inequality is also checked within the whole region, and the red spot at the left side of the figure shows the region which does not meet Eq.10. Considering the suitable region specified by the constraint, the optimal solution should have a GCI closer to 1. Additionally, to minimize the total length of the linkages, l and a should be chosen to be as small as possible. It is to be noted that we have also a limit on the negative values of a as it requires a complex design of the rotating arm. Considering all the discussion herein, we have chosen $a = 0.024$(m) and $l = 0.110$(m) for which $GCI = 0.49$ for the implementation of the robot.

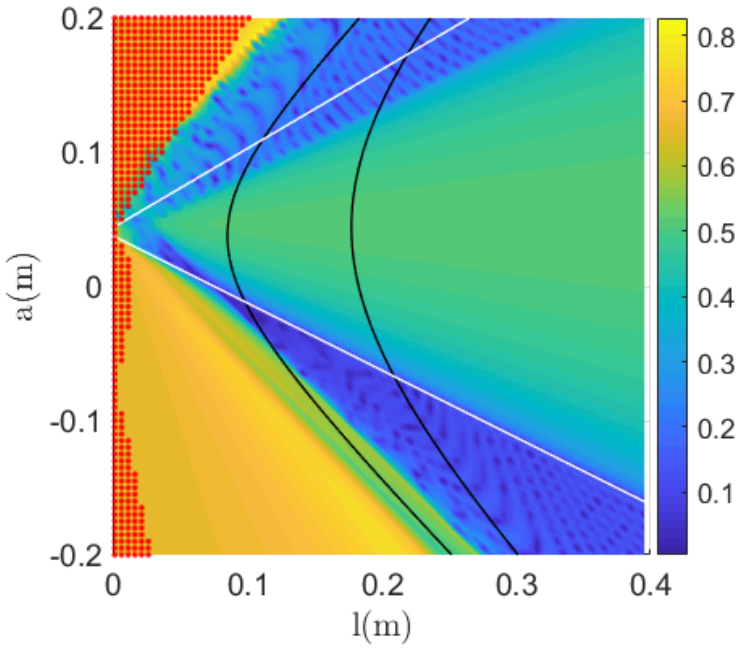

Figure 2.8: Global inverse condition number of the parallelogram mechanism as a function of a and l within the whole flexion/extension range, considering the kinematic constraints in (9), (10), (11).

2.5 Kinematic Validation

To verify the kinematics of the robot, the robot model is simulated in MATLAB Simscape. A periodic trajectory is first given to the kinematic model in the task space (reference trajectory ϕ_r and θ_r) to obtain the corresponding joint space variables. The obtained values for the joint variables are given to the Simscape model, and the resultant task space variables ϕ and θ are compared to the original trajectory. The trajectory error for both ϕ and θ in kinematic validation is shown in Fig.

2.9. The error is less than 0.025° for both ϕ and θ.

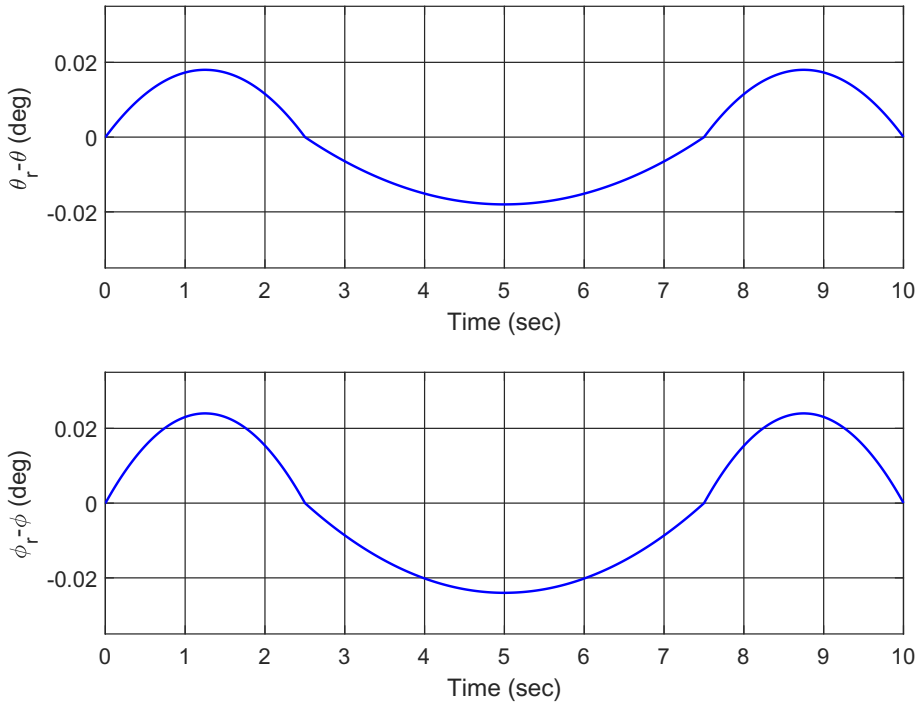

Figure 2.9: Kinematic validation: errors of θ and ϕ motions.

2.6 Implementation

Based on the mechanical design and kinematic optimization explained in section 2.3 and 2.4, a prototype of the robot is developed using 3D printing technology, as shown in Fig.2.10. The total mass of the robot including the actuators and the two supports at the ends is 1.3 kg. The length parameters of the implementation setup are also depicted in Table 2.3.

Table 2.3: Mechanism parameters

Parameter	a	b	l	d	AB	δ
Quantity (mm)	24	75	110	230	170	20

Based on the mechanical design, the rotating arm is mounted on two bearings at either of its ends. The rotation of the base is provided using a servo motor connected to a helical pinion gear.

A partial helical gear is also integrated at the rotating arm, which receives rotation from the pinion gear connected to the servo motor. The parallelogram mechanism is mounted on the rotating arm, and its motion is provided using a nut mounted on a lead screw. The lead screw pitch is 2mm, and it has four flutes which cause the nut to move 8mm per revolution. The lead screw also works as the shaft of the rotating arm and is mounted on two sets of bearing on both the rotating arm as well as the fixed supports. The lead screw is coupled to the corresponding servo motor using a spring coupling. The nut of the lead screw is connected to a part that is mounted on a linear guide at the bottom of the rotating arm. Rotating the lead screw causes the nut to move back and forth. Thus, the parallelogram mechanism moves up and down and provides the flexion/extension motion of the patient wrist. Additionally, with the rotation of the gear attached to the rotating arm, the whole structure of the mechanism rotates about the lead screw axis and moves the patient wrist in radial/ulnar direction. As discussed earlier, this motion also provides flexion/extension motion which can be simply compensated using the kinematic equations.

Figure 2.10: A 3D printed prototype of MOCH.

To have a stiff structure and minimizing joint backlash, two identical mechanisms are coupled to each other. The links of the mechanism are connected to each other as well as to the rotating arm using miniature bearings. The distal links of the mechanism are modified to be used as the robot

end-effector by the patient. Once the patient holds the end-effector, the RCM of the mechanism coincides with the center of rotation of the wrist, allowing pure rotation about the RCM point.

2.7 Experimental Results

In the passive rehabilitation practice, the muscles are in rest, and the therapist moves the wrist of the patient within the ROM. To verify the effectiveness of the proposed design, the experimental setup has been evaluated for both flexion/extension and radial/ulnar motions for passive exercises. To aim this, a periodic trajectory is designed, starting from the neutral position (i.e. $\theta = 90$ and $\phi = 0$) of the hand. It is to be noted that the given trajectory to the patient hand should not violate the maximum allowable torque in the wrist. Considering this fact we have been working on a methodology for optimal trajectory generation, considering human hand dynamics described in Eq.(1). It is to be noted that trajectory design is not in the scope of this chapter and we just use the result of optimal trajectory. Knowing the kinematics of the robot the desired trajectory in the task space, the joint space trajectory is obtained for the actuators. The actuators are servo motors with inner PID controllers. The tracking performance of the robot in the workspace based on the actuator rotary sensors is given in Fig. 2.11 and Fig. 2.12. It is to be noted that these figures are provided based on the hand coordinate in which the neutral position of the hand is where $\theta = 90^\circ$.

As it is clear from Fig. 2.11 and Fig. 2.12 the maximum tracking errors are less than $\pm 0.5^\circ$ and $\pm 0.2^\circ$ for flexion/extension and radial/ulnar motion, respectively. It is to be noted that the given trajectory in this experiment is just for the verification of the robot performance which was obtained for certain parameters of the wrist and is not suggested for rehabilitation exercise. Verification of the proposed trajectories requires clinical experiments and approval of the governing organizations.

As discussed the given trajectory to the robot is based on an optimization method using dynamics of the hand. For a better clarification and verifying the safe operation of the robot when interacting with the patient, the applied torque to the hand is found using the inverse dynamics of the hand given by equation (1). Figures 2.13 and 2.14 show the wrist torque during the passive rehabilitation exercise. As shown in the figures the maximum value of the torques lies within the limits of the wrist strength specified in [49, 50]. It is to be noted that these torques are defined based

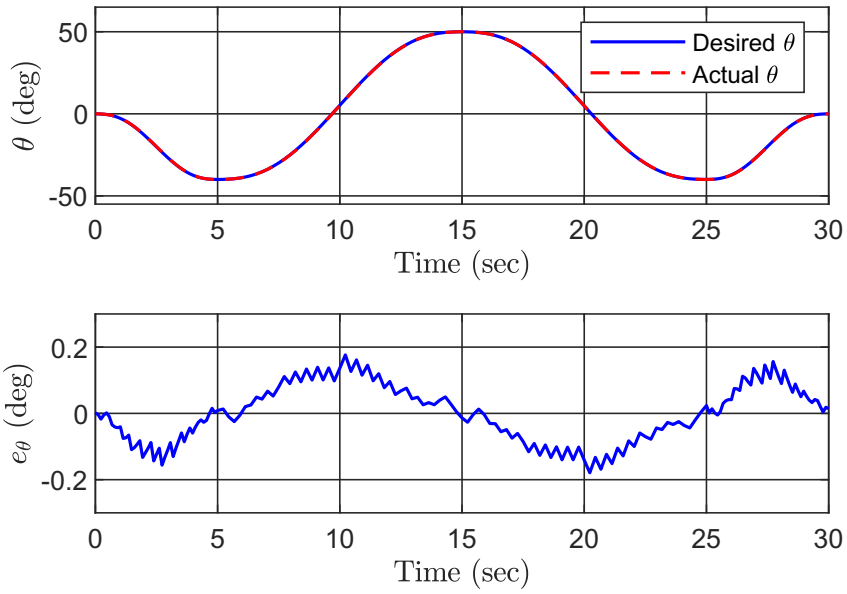

Figure 2.11: Trajectory tracking performance for flexion/extension motion when $\phi = 0$.

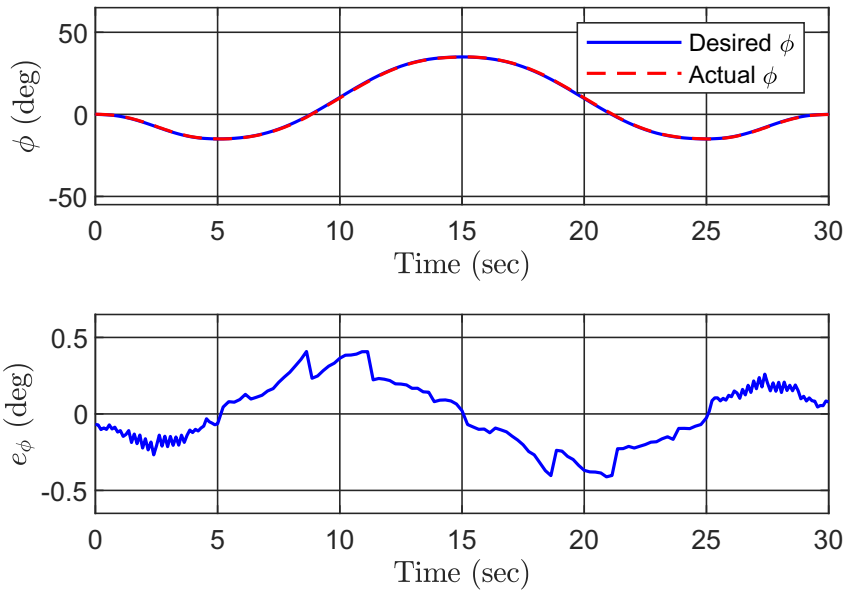

Figure 2.12: Trajectory tracking performance for radial/ulnar motion when $\theta = 90°$

on the hand coordinate system. As the actuators are supposed to generate the required trajectory for the hand there would be some errors for the torques which is also depicted in the figures, denoted by $e_{\tau\theta}$, $e_{\tau\phi}$. The mean square of the torque tracking errors for the experiment along with the position and torque tracking is summarized in Table 2.4.

Table 2.4: Position and torque tracking error (SI units)

Parameter	θ	ϕ	τ_θ	τ_ϕ
RMSE	0.085	0.196	0.012	0.004

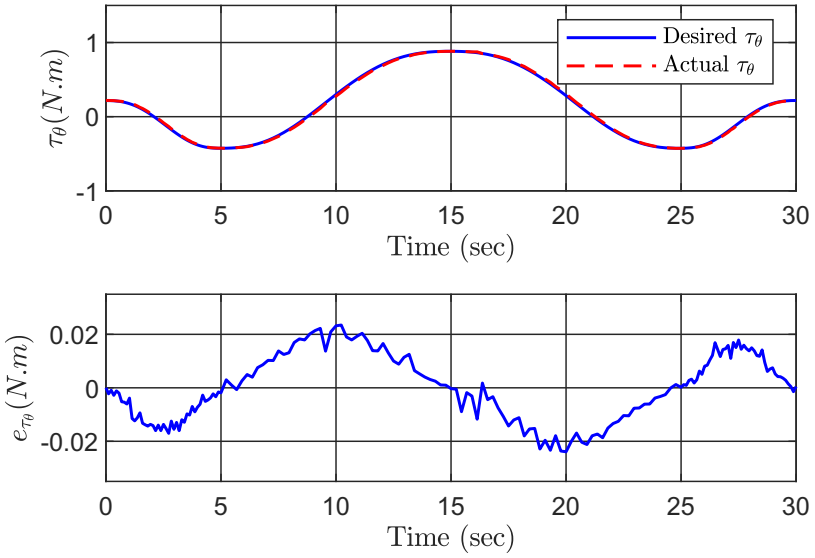

Figure 2.13: Torque tracking performance for flexion/extension trajectory when $\phi = 0$.

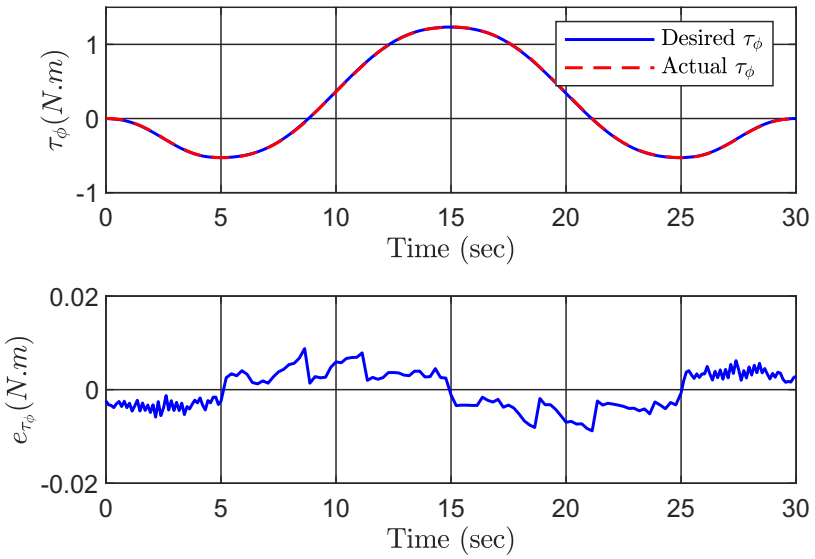

Figure 2.14: Torque tracking performance for radial/ulnar motion when $\theta = 0$.

2.8 Summary

In this chapter, a robot for wrist rehabilitation, referred to as MOCH was introduced, which offers portability, and a low-cost simple manufacturing process. The novel actuation proposed in this study allowed us to position both of the actuators at the base which simplifies the design and removes the complexity for feeding power to actuators on rotating arm. The handle of the robot can be easily held by the user while the robot is in motion in both directions. The developed prototype of the robot verifies the design requirements experimentally, as well as being inexpensive for low-budget patients for home use. It also shows reliable tracking performance for passive wrist rehabilitation exercises. The implemented robot is the first prototype of MOCH for passive rehabilitation practice. We plan to improve the design for active rehabilitation exercises, by adding a series elastic actuation and replacing gear transmission with capstan-drive. This upgrade will help us to further investigate the performance of the robot with impedance, stiffness, and force control schemes for active exercises.

A variety of trajectories can be given to the robot but as in rehabilitation, there is an interaction between the robot and human, safety in trajectory design must be considered. Trajectories needed to be designed and optimized to guarantee that the applied interaction torque does not hurt the human wrist. This goal leads us to the next chapter which introduces a new idea for designing a safe trajectory based on the dynamics of the human wrist. The governing equation of human wrist dynamics is solved with several constraints and limits in the amount of torque exerted on the wrist using an open source optimization toolbox. Then the optimized trajectories are converted to joint space trajectories using inverse kinematics and the joint space trajectories are then given to the servo motors.

Chapter 3

Optimal Trajectory Planning for Wrist Rehabilitation

The impairment of the upper limb is one of the most common stroke consequences. Robotic rehabilitation provides a potential way to regain functional movements for those who have such disabilities. Robots used for upper limb rehabilitation are usually end-effector-based robots and wearing robotic orthoses. Most of the current designs for the end-effector-based robots have three degrees of freedom and are built on an open kinematic chain. This characteristic results in a bulky structure and there is a high risk of interfering with the patient's hand, which can be dangerous. Also, most of these robots are equipped with force sensors at the contact point with the patient's hand to make sure that the exerted force applied on the hand is in a safe range. However, integrating the force sensors is costly and adds to the complexity of the operation. In this chapter, we introduce a novel wrist rehabilitation robot based on a remote center of motion mechanism, referred to as MOCH. The center of rotation of this mechanism lies outside of the robot structure, which eliminates the risk of interference with the patient. The proposed design is portable, inexpensive, and lightweight, with its compact size and actuators at the base.

Additionally, We introduce a novel methodology for passive rehabilitation exercise, exploiting the wrist dynamics which removes the complexity of force/impedance control approaches. This method involves designing safe optimal trajectories in terms of applied torque on the patient's hand,

considering the limits in the range of motion to keep the interaction force with the robot in a safe range. The proposed method removes the integration of force sensors which generally is costly and removes the complexity of the robot.

3.1 Introduction

Globally, stroke is among the main causes of death and disability [1]. Over 80 million individuals have already suffered a stroke in their lifetime and over 13.7 million new cases are reported each year [1]. More than 5.5 million of these new cases result in death while the rest show impairment of the limbs [1]. Studies have shown that early rehabilitation therapy after a stroke has a major impact on the treatment and recovery process [2]. Physical rehabilitation treatment is a long procedure and the results usually appear as early as six months after the therapy begins [2]. In order to maximize recovery, rehabilitation therapy requires continual repetition, which makes it a costly service for patients [3], [4]. Due to this, it is beneficial to use robots for rehabilitation therapeutic services. Many types of applications, including rehabilitation therapy, are being automated with robotics. There is an increasing trend of using robots in rehabilitation therapies. MIT-MANUS is one of the most renowned robots of its kind designed and developed for upper limb rehabilitation [5]. A SCARA planar mechanism with two DoF aiming shoulder and elbow motions is used in the MANUS first prototype. An improved version of MANUS has a wrist and forearm robot module capable of moving in three degrees of freedom [51], [6]. Since the robot is going to have to interact with the human hand, an impedance control scheme is used to adjust the robot's compliance [5].

Lum et al. created a system called MIME to assist in shoulder and elbow rehabilitation, utilizing a 6 DoF industrial PUMA serial robot [7], [8]. The patient's forearm is fixed to the robot end-effector and the interaction forces and torques between the robot and patient are measured using a 6 axis sensor [9]. The robot moves the forearm according to the defined trajectory in the space and an embedded PID controller of the robot is used for tracking this trajectory. The positive effect of using MIME in rehabilitation therapy comparing to usual therapies was demonstrated in a clinical trial [9]. A robot named ARM Guide was introduced and developed by Reinkensmeyer et al. to improve arm disabilities after brain injuries [52], [11]. It moves the patient's forearm linearly along

a guide using its 1 active DoF [52]. A counterweight is used to compensate the whole arm and hand weight and a PID control scheme is implemented to track the designed trajectory and help the patient to complete the movement [10].

A 6 DoF robot named ARMin which aims at rehabilitation of arm impairments was introduced [12]. The robot is equipped with several position, speed, and torque sensors and is able to do four various control strategies [12]. Firstly, the rehabilitation process done by a professional therapist can be recorded, and then the robot can repeat it [12]. Secondly, the robot can do several defined trajectories on the patient [12]. Thirdly, for patients who can't move their hands, the robot can help them to do predefined movements [12]. Fourthly, when the patient moves his/her hand, the robot tries to estimate the forces and torques and does a portion of them to help him/her [12]. The position control scheme is used for the first two ones and the impedance control scheme is applied for the last two ones [12]. By adding more degrees of freedom to ARMin, ARMin II was introduced which in comparison to the first version has more complicated maneuvers. ARMin II has 7 DoF which causes patients to feel more comfortable during therapy [13].

A rehabilitation device designed specifically for the forearm and wrist named Bi-Manu-Track is developed by Hesse et al. [14]. There are 2 degrees of freedom in total in this device, with one dedicated to the wrist and the other to the forearm [14]. The patient's hands are placed within two ergonomic parts, strapped and fastened with bands, while sitting at a table. It is possible for the therapist to adjust the rotation angle, speed, and torque from the control panel [15]. There are two types of handles for the device which have to be demounted and remounted in order to switch from flexion/extension to pronation/supination. [15]. Having a simple structure and the ability to practice rehabilitation exercises on both hands at once are great features of this device [15]. Different control schemes such as position and compliance control are used for this robot. In a clinical study involving several patients, motor function improvement was observed after a short period of the robot use [14].

The Wrist Gimbal robot, developed by Martinez et al. has 3 degrees of freedom [22]. It covers the wrist and forearm motions and has two modes for controlling including passive mode and resistive mode [22].

The CDWRR robot designed by Cui et al. is used for rehabilitation of the forearm and wrist. [25]. A handle attached to the robot is suspended from four cables and the length of each cable is

controlled by a separate motor. Shortening or extending these cables gives the robot three degrees of freedom for the wrist and forearm [26]. To help the patient achieve a defined task trajectory, it uses a torque-field controller which provides necessary forces [26].

This chapter discusses a novel approach towards trajectory design for controlling our two DoF portable rehabilitation robot named MOCH. Trajectories must be designed to avoid any damage to the patient's hand as it interacts with the rehabilitation robot. This is achieved through the use of a position control with a torque limit on the motors to ensure the safety of wrist and robot interaction. To reach this goal, a method was used based on the existing dynamical model of the human wrist which will be explained in detail.

3.2 Control Schemes

One of the essential aspects of the rehabilitation robot is the control architecture. A suitable control scheme for a wrist rehabilitation robot should move the patient's hand on a reference trajectory while keeping the interaction force with the wrist within the acceptable threshold. These control paradigms could be divided into two main categories, namely position control (position trajectory tracking) and force control [53].

3.2.1 Position Control

In the position control scheme, the robot moves the patient's hand on a predefined trajectory, which can be obtained from the actual therapy. In this scheme, the contact force/moment can reach very high values causing damage either to the manipulator or the environment.

3.2.2 Force Control

In the force control scheme, the robot moves the patient's hand in a predefined position trajectory as well as tracking a desired interaction force trajectory. There are several force control schemes including direct force control, stiffness control, and impedance control. In direct force control, there is a force feedback in the control scheme by using a force sensor placed at the contact point of the robot and environment which allows the controller to track the predefined force trajectory [54]. In

the stiffness control scheme, the interaction force between the robot and the environment is kept in a safe range by establishing a relation between the force and movement of the robot end-effector and environment. Choosing the right controller gain is very important in this control method. [54]. The impedance control scheme was initially proposed by Hogan [55] for safe interaction of the robots with the environment, by establishing a dynamic relationship between the force and velocity of the robot.

3.3 Optimal Trajectory Planning

In human-robot interaction, the force interaction is a major playing role. To ensure safe interaction with the human, the interaction force should be managed to prevent damage. Force control scheme requires relatively complex control architecture as well as force feedback which adds to the complexity and the final cost. Additionally not all the actuation systems are suitable for force control and it demands specific mechanical design. The proposed design of the wrist rehabilitation robot in this chapter is based on leadscrew linear actuators and we are using simple servo motors for the actuation. To make use of such a kind of robot for human-robot interaction, we need to have a precise understanding of the interaction environment, which in our case is the dynamics of the human wrist. While having the dynamic model, with a given trajectory we can find the induced force in the wrist. Being so, we investigate optimal trajectory planning to design a suitable trajectory for the human wrist motion while keeping the interaction force with the wrist in a safe threshold and at the same time meeting the joint limits which will be later discussed in detail.

3.3.1 Wrist Kinematics

As it is demonstrated in Fig. 3.1 human wrist has 2 types of motions named flexion/extension and radial deviation/ulnar deviation. So from a mechanical perspective, it is a 2 DoF universal joint and has 2 axes of rotation. ROM (Range of Motion) of the human wrist is a parameter that is required for designing the rehabilitation robot as the robot has to cover these motions.

It has to be considered that joints never reach their maximum ROM in human daily activities so the functional ROM is less than the maximum ROM. For this reason, most rehabilitation robots use

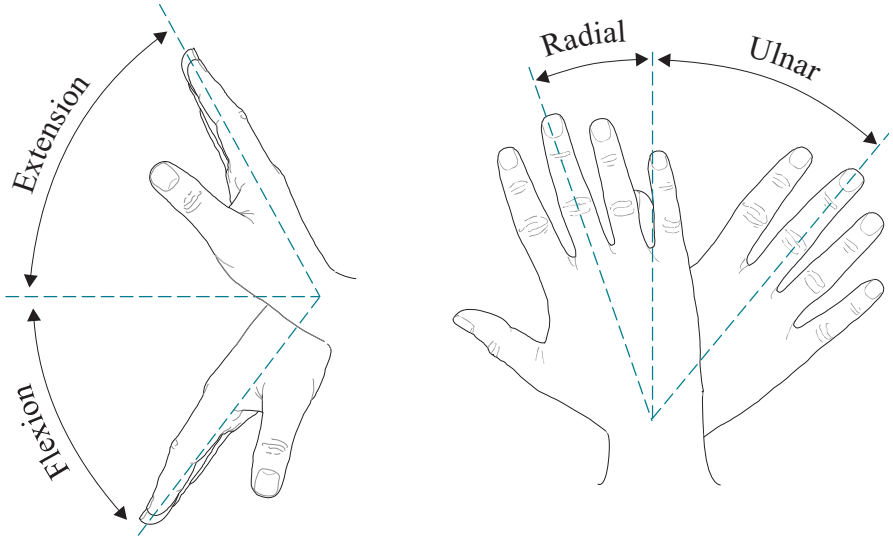

Figure 3.1: Wrist motions and degrees of freedom.

ADLs (Activities of Daily Living) ROM instead of ROM in the therapies. The table 3.1 shows the ADLs ROM of the wrist measured by [44].

Table 3.1: Wrist ADLs ROM

Motion type	ADLs ROM
Flexion-Extension	$-54°$ to $60°$
Radial-Ulnar	$-17°$ to $40°$

3.3.2 Dynamic Model of the Wrist

Considering the wrist as a universal joint, the governing dynamic model of the wrist rotation can be expressed as the following equation [46]. In the equation, θ and ϕ show the rotations around the wrist center of rotation for the flexion-extension and radial-ulnar directions, respectively. τ_θ and τ_ϕ are the torques generated in the wrist for θ and ϕ directions, respectively. Also, m is the mass of the hand, and r is the distance between the center of the mass of the hand and the wrist center of rotation.

$$\begin{bmatrix} \tau_\theta \\ \tau_\phi \end{bmatrix} = \begin{bmatrix} I_\theta & 0 \\ 0 & I_\phi \end{bmatrix} \begin{bmatrix} \ddot{\theta} \\ \ddot{\phi} \end{bmatrix} + \begin{bmatrix} C_\theta & C_{\theta\phi} \\ C_{\theta\phi} & C_\phi \end{bmatrix} \begin{bmatrix} \dot{\theta} \\ \dot{\phi} \end{bmatrix} + \begin{bmatrix} K_\theta & K_{\theta\phi} \\ K_{\theta\phi} & K_\phi \end{bmatrix} \begin{bmatrix} \theta \\ \phi \end{bmatrix} + \begin{bmatrix} mgr\cos\theta \\ 0 \end{bmatrix} \tag{14}$$

Referring to the equation above, the dynamics of the wrist depends on the mass (m), inertia (I), stiffness (K), and damping (C) of the wrist, however, most of the studies consider stiffness as the dominant part of the dynamics. The parameters of the wrist have been measured in experimental studies and vary from one person to another. The inertial parameters are relatively simple to measure, comparing to stiffness and damping, and we use those values reported by Charles and Hogan, [46]. The stiffness of the wrist is configuration dependant [46] and most of the studies are based on the linear approximation in a limited range of motion (ROM). In our study, we use those values reported by Pando et al. [45] as the measurements are for larger ROM and which covers 70 percent of the daily living activities (ADLs). As most of the dynamic effects of the hand depend on the stiffness, there are limited studies for the damping measurement. In [46], the authors have assumed that the damping ellipse has the same shape and orientation as the stiffness ellipse and based on this assumption and their measurements, they have proposed 5 percentage of the stiffness for the damping. The chosen values for the parameters are summarized in the Table 3.2.

Table 3.2: Dynamic parameters of the wrist [46]

Inertia (kgm^2)	Stiffness (Nm/rad)	Damping (Nm/rad^2)	Gravity effect ($N.m$)
$\begin{bmatrix} 0.0022 & 0 \\ 0 & 0.0022 \end{bmatrix}$	$\begin{bmatrix} 0.85 & -0.27 \\ -0.27 & 2.02 \end{bmatrix}$	$\begin{bmatrix} 0.043 & -0.014 \\ -0.014 & 0.101 \end{bmatrix}$	$\begin{bmatrix} 0.218 \\ 0 \end{bmatrix}$

The maximum strength or torque of the wrist for flexion/extension and radial/ulnar deviation is a factor that is needed for designing safe trajectories. There are many studies focusing on the measurement of wrist strength. We have considered the flexion/extension strength measured by Decostre et al. [49] and radial/ulnar deviation strength measured by Dianat et al. [50] as these studies have a large number of test participants including both sexes of different ages.

3.4 Trajectory Optimization Problem

Our goal is to design trajectories for θ and ϕ to make sure that the torque generated in a human's wrist by these trajectories is in the safe range and does not damage the wrist. This problem

can be formed as an optimization problem in order to choose one trajectory among many feasible trajectories which can be represented in a general form as:

$$\begin{aligned} \min_{\boldsymbol{x},\boldsymbol{u}} & \int_0^{t_f} w(t,\boldsymbol{x}(t),\boldsymbol{u}(t))\,dt \\ \text{s.t.} \quad & C^{eq}(t,\boldsymbol{x}(t),\boldsymbol{u}(t)) = 0, \\ & C^{ineq}(t,\boldsymbol{x}(t),\boldsymbol{u}(t)) \leq 0. \end{aligned} \tag{15}$$

where $\boldsymbol{x} = \begin{bmatrix} \theta & \phi & \dot{\theta} & \dot{\phi} \end{bmatrix}^T$ is the state vector and $\boldsymbol{u} = \begin{bmatrix} \tau_\theta & \tau_\phi \end{bmatrix}^T$ is the control input vector. C^{eq} is the set of equality constraints, and C^{ineq} is the set of inequality constraints. $w(t, x_t, u_t)$ is the objective function which is needed to be minimized.

Objective function: For finding the optimal trajectory, we have to find out which objective function is suitable to be minimized for this task [56]. Different types of objective functions were tested and finally, the total squared acceleration $w(t, x_t, u_t) = (\ddot{\theta}^2 + \ddot{\phi}^2)$ was chosen as an objective function because in rehabilitation sudden change in velocity is not recommended.

Equality constraints: C^{eq} includes the initial and final conditions where a trajectory for θ and ϕ starts and ends with zero velocity.

$$\begin{aligned} \theta(0) = 0, \theta(t_f) = \theta_f \\ \phi(0) = 0, \phi(t_f) = \phi_f \\ \dot{\theta}(0) = 0, \dot{\theta}(t_f) = \dot{\theta}_f \\ \dot{\phi}(0) = 0, \dot{\phi}(t_f) = \dot{\phi}_f \end{aligned} \tag{16}$$

System dynamics $\dot{\boldsymbol{x}} = f(\boldsymbol{x}, \boldsymbol{u})$ is also part of C^{eq} which can be obtained from the wrist forward dynamics as

$$\begin{bmatrix} \ddot{\theta} \\ \ddot{\phi} \end{bmatrix} = \begin{bmatrix} I_\theta & 0 \\ 0 & I_\phi \end{bmatrix}^{-1} \left(\begin{bmatrix} \tau_\theta \\ \tau_\phi \end{bmatrix} - \begin{bmatrix} C_\theta & C_{\theta\phi} \\ C_{\theta\phi} & C_\phi \end{bmatrix} \begin{bmatrix} \dot{\theta} \\ \dot{\phi} \end{bmatrix} - \begin{bmatrix} K_\theta & K_{\theta\phi} \\ K_{\theta\phi} & K_\phi \end{bmatrix} \begin{bmatrix} \theta \\ \phi \end{bmatrix} - \begin{bmatrix} mgr\cos\theta \\ 0 \end{bmatrix} \right) \tag{17}$$

Inequality constraints: C^{ineq} includes box constraints on joint torques. Considering the maximum allowable torque limits obtained by Decostre et al. [49] and Dianat et al. [50], the limit 1.5 (N.m) was selected for both torque constraints.

$$
\begin{aligned}
|\tau_\theta| &\leq 1.5(N.m) \\
|\tau_\phi| &\leq 1.5(N.m)
\end{aligned}
\tag{18}
$$

Software tool: We solve the optimal control problem with the open-source toolbox developed by Kelly [56] which is based on the direct collocation method. The solver requires an initial guess where a fifth-order polynomial with zero velocity and acceleration at the initial and final time is applied. In this method, the continuous functions are discretized by approximating all functions as polynomial splines.

Fig. 3.2 shows the optimized trajectory for the θ direction when ϕ is in a neutral position and is equal to zero. It is the output of the collocation method and a cycle starting from a neutral position. Fig. 3.3 demonstrates the output of the collocation method for ϕ when θ is neutral. As it is clear

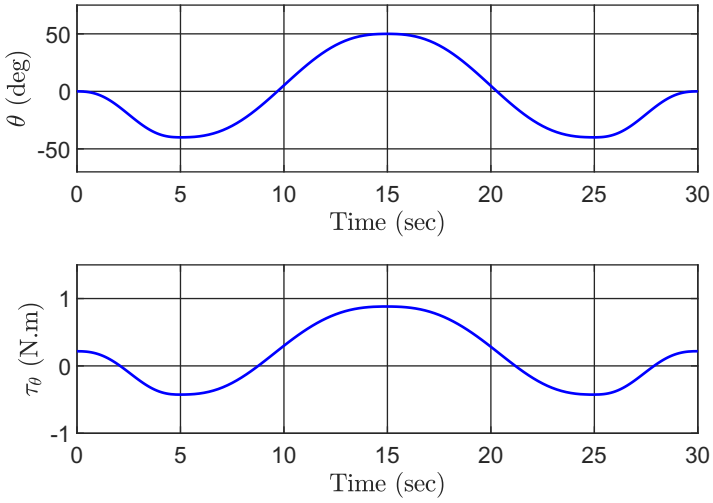

Figure 3.2: The designed trajectory for θ and the torque applied to the wrist due to this trajectory.

the amount of torque generated in the wrist due to trajectories is in the safe range in both cases. Fig. 3.4 shows the trajectory designed using the collocation method when both θ and ϕ change simultaneously In Fig. 3.5 the equivalent 3D path of the human hand's center of mass for the

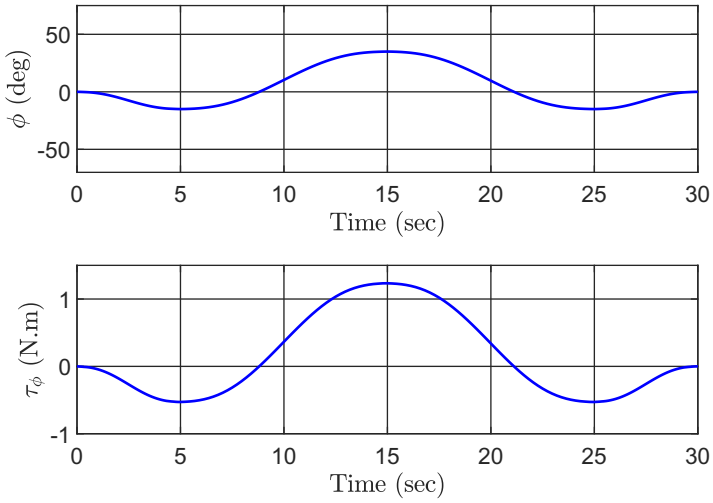

Figure 3.3: The designed trajectory for ϕ and the torque applied to the wrist due to this trajectory.

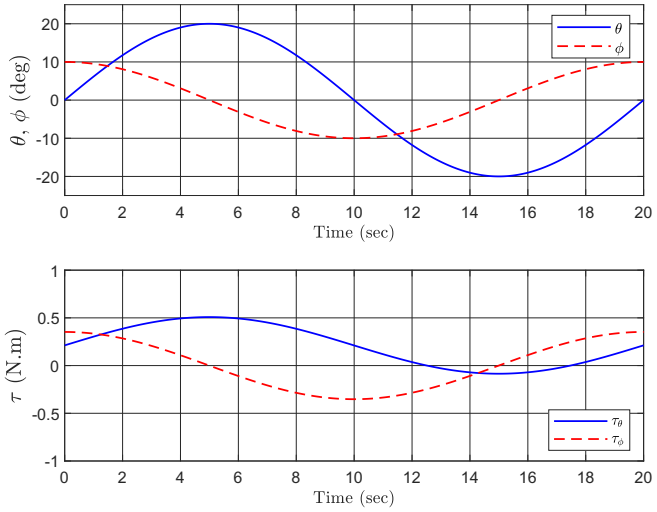

Figure 3.4: The designed trajectory for θ and ϕ and the torque applied to the wrist due to this trajectory.

combined trajectory (when both θ and ϕ change together) can be seen.

3.5 Experimental Setup

Fig. 3.6 shows the CAD model of the designed robot and its interaction with the patient hand. There are two servo motors in the robot that provide two degrees of freedom, and both of them are mounted at the base. A self-aligning coupling is used to couple one of them to a lead screw.

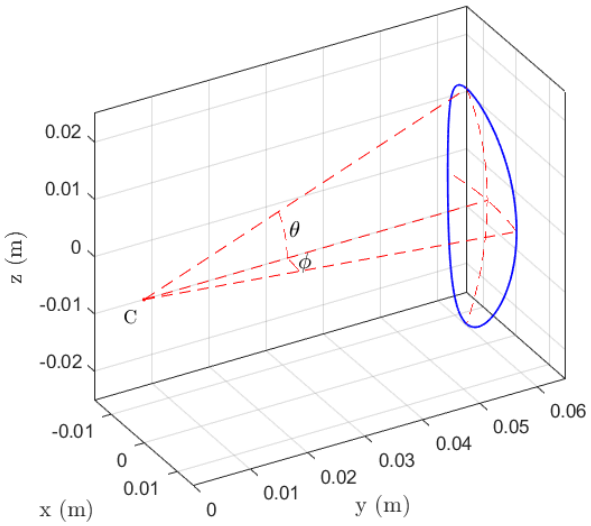

Figure 3.5: 3D path when θ and ϕ change together.

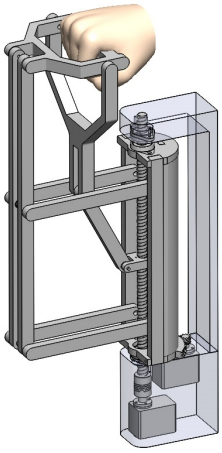

Figure 3.6: CAD model of MOCH.

Each end of the lead screw has two sets of self-aligning bearings. Two of them hold the lead screw in place while the other two let the whole parallelogram rotate about the lead screw axis. A nut connected to the coupling link of the robot moves back and forth when the lead screw is rotated. As a result, the parallelogram mechanism moves up and down and causes the patient's wrist to do a flexion and extension motion. The nut is connected to a linear guide in order to move in a straight line. The second servo motor drives a helical pinion, which is in contact with a larger helical gear. As this larger gear rotates, the entire mechanism revolves around the lead screw axis, so the patient's wrist does radial and ulnar movements. As this motion does not require full rotation, the larger gear

Figure 3.7: A 3D printed prototype of MOCH.

is a sector gear. For greater stability, more symmetry, and strength, two parallelograms are placed next to each other. Small ball bearings are used to connect links of the parallelogram together, minimizing friction and enabling a smoother motion. As shown in Fig. 3.7 the robot interacts with the patient's hand through a designed handle.

3.6 Results

The optimized trajectory is given to the robot servo motor as the desired trajectory for observing the tracking performance and error. Also, the output position is read from the servo motor encoder and is named as actual trajectory. Fig. 3.8 shows these two desired and measured position trajectories together in one graph for θ. It also shows the tracking error between these to position trajectories for θ angle. The error is less than 0.2 degrees. Fig. 3.9 shows the same results for ϕ angle when θ is in a neutral position. As it can be seen the tracking error is less than 0.5 degrees.

The measured position trajectory from the servo motor encoder is given to the dynamics of the wrist to compare the generated torque in the wrist with the output torque of the optimization. Fig. 3.10 shows the result for θ direction and as it is clear that the two torque profiles are approximately equal to each other and the difference between them is less than 0.02 N.m. Fig. 3.11 shows the same results for the ϕ direction. As it demonstrates, the tracking error is less than 0.01 N.m.

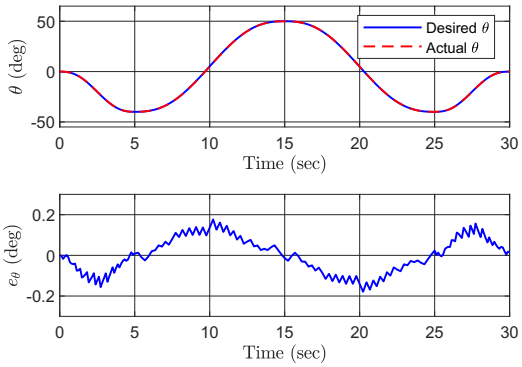

Figure 3.8: Trajectory tracking performance for flexion/extension motion when $\phi = 0$.

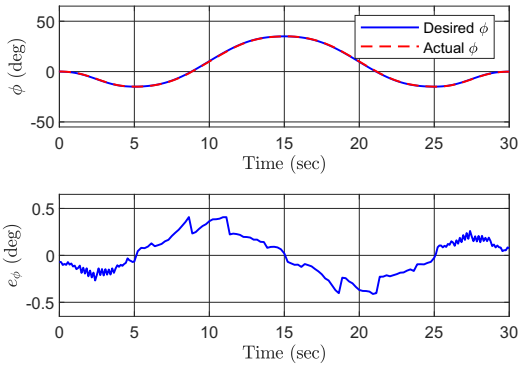

Figure 3.9: Trajectory tracking performance for radial/ulnar motion when $\theta = 90°$

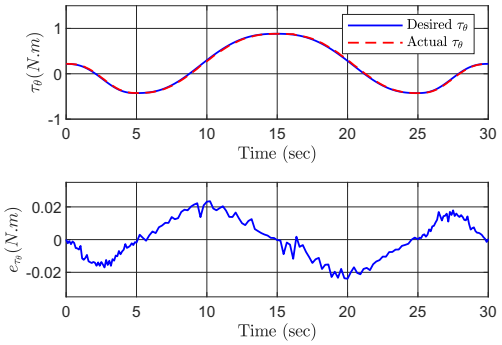

Figure 3.10: Torque tracking performance for flexion/extension trajectory when $\phi = 0$.

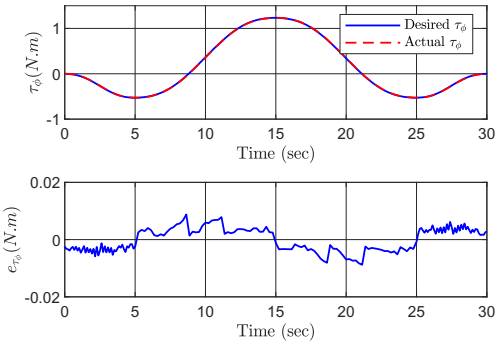

Figure 3.11: Torque tracking performance for radial/ulnar motion when $\theta = 0$.

3.7 Summary

In this chapter, a newly designed wrist rehabilitation robot called MOCH was introduced. The actuation system of the robot is novel which makes the robot structure simple as the actuators are fixed at the ground. Also, a novel approach in designing and optimizing the trajectory for the wrist rehabilitation robot was introduced. Dynamic equations of the human wrist were solved and optimized numerically with the collocation method to satisfy constraints in torque and position. Total acceleration was considered as an objective function and it was minimized for obtaining the optimal trajectory in both directions.

Chapter 4

Drawings, Fabrication, Experimental Setup and Testing

4.1 Introduction

In this chapter, the details of the robot structure and its different mechanical parts with their dimensions will be demonstrated through drawings. Also, the manufacturing process of the mechanical parts will be explained. The elements of the experimental setup will be shown and the testing procedure on a healthy person will be explained.

4.2 Drawings

To have a better understanding of the robot, different parts of the robot with detailed drawings are demonstrated. Fig. 4.1 shows the total dimensions of the robot and its bounding box in the space. Fig. 4.2 shows the actuation mechanism of the robot for ϕ angle. The servomotor is responsible for making the ϕ angular motion of the robot. The servomotor rotates the designed 3D printed pinion gear and the pinion gear which is in contact with a helical sector gear causes the whole rotating arm and parallelogram to rotate around the lead screw axis.

In Fig. 4.3 the actuation of the robot for θ angle is seen. The servomotor is responsible to rotate the lead screw and make the θ angular motion of the robot. The servomotor is connected to the

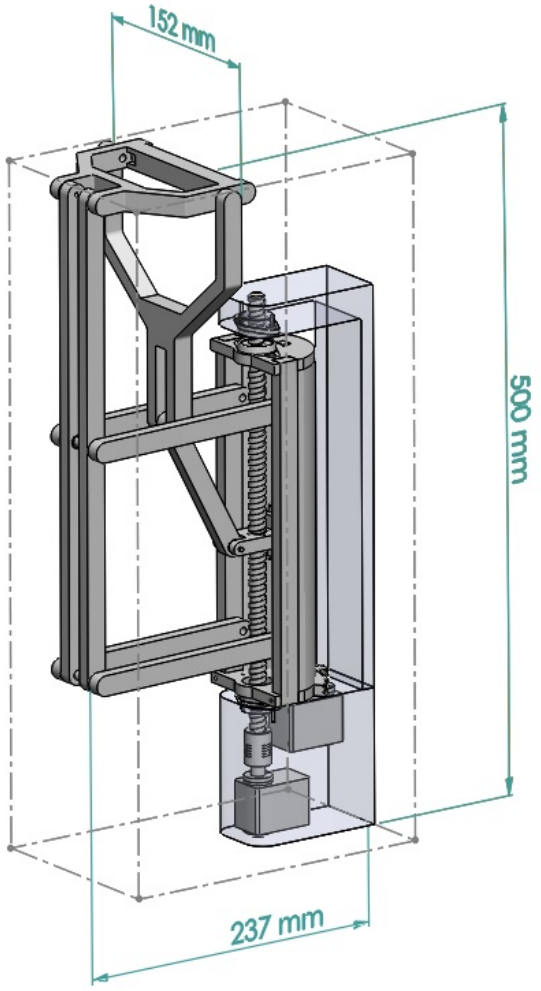

Figure 4.1: The robot dimensions.

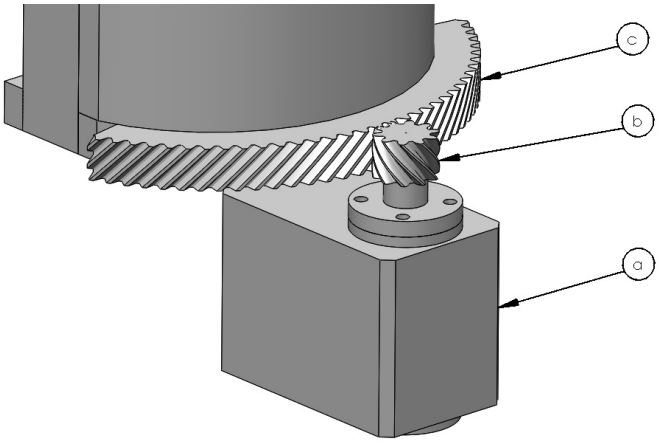

Figure 4.2: (a) Servo motor for ϕ angle (b) pinion gear (c) Helical gear.

coupling using a designed connection part as the motor shaft diameter is different from the coupling inner diameter. A flexible coupling is selected for the connecting to the lead screw to cover any probable misalignment. The lead screw itself relies on the bearings.

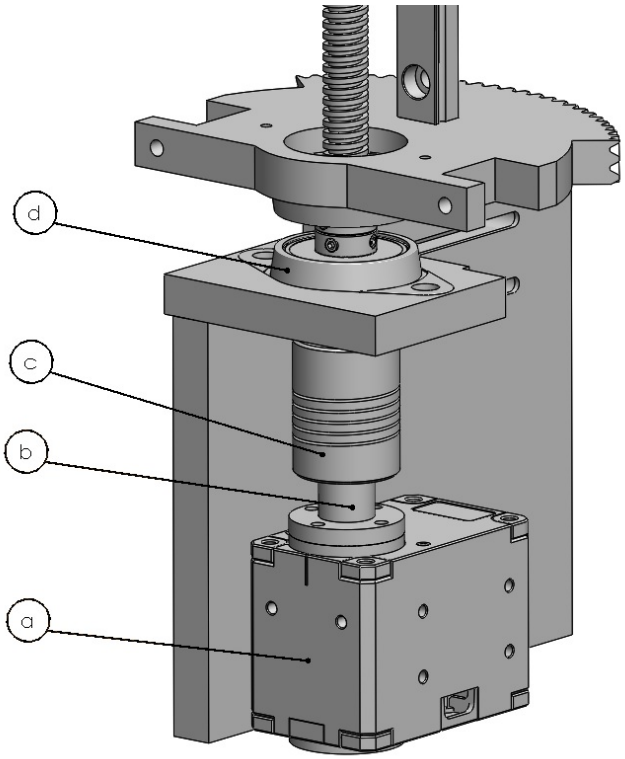

Figure 4.3: (a) Servo motor 1 for θ angle (b) connection part between the motor and coupling (c) spring coupling (d) bearing.

Fig. 4.4 demonstrates the linear motion mechanism of the robot. The servo motor which is responsible for θ movement rotates the lead screw and this causes the linear movement of the nut. As the nut is fixed to the designed connection part, it can not rotate and just moves along the lead screw axis. Using the rail and carriage prevents the nut from rotating and helps us to have a straight linear motion. Some of the important mechanical parts of the robot will be explained in detail below.

4.2.1 Spring Coupling

For connecting the servo motor 1 to the lead screw, a spring coupling is used because it is flexible and can compensate for any kind of misalignment which may happen between the shaft axis of the servo motor and the lead screw axis during the assembly of the robot parts. The spring coupling

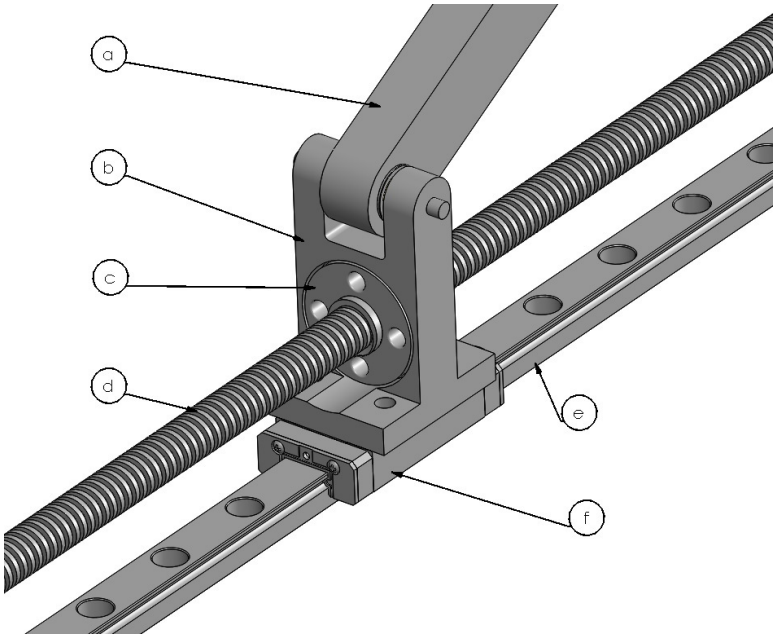

Figure 4.4: (a) Coupling link (b) connection part between the nut and carriage (c) nut (d) lead screw (e) rail (f) carriage

on one side has an 8mm hole in which lead screw goes into it and a small adjustment screw on the coupling prevents the lead screw from slipping inside the coupling hole. Fig. 4.5 shows the spring coupling and its dimensions.

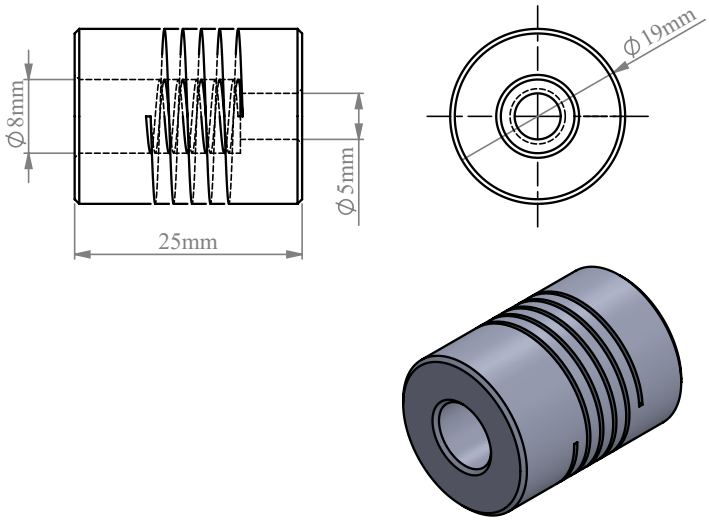

Figure 4.5: Spring coupling

4.2.2 Connection Part between the Motor and Coupling

As the motor flange can not be connected to the coupling directly, a mechanical part is needed to be designed to connect them together. From one side, it is connected to the motor flange with 4 screws and the other side goes inside the coupling and is locked with an adjustment screw on the coupling. Fig. 4.6 shows this designed and 3D printed part and its dimensions.

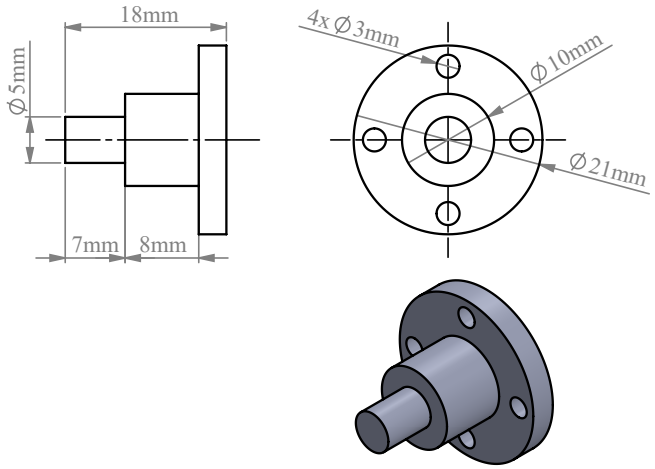

Figure 4.6: Connection part between the motor and coupling

4.2.3 Pinion Gear

Fig. 4.7 shows the pinion gear which is designed and 3D printed for connection to the servo motor 2 which generates the ϕ rotation of the robot. The type of this pinion gear is helical because helical gears make less noise comparing to spur gears. This part also has a flange that sits on the servo motor flange with four screws. The pinion gear has 10 teeth and is in contact with the bigger helical gear.

4.2.4 Helical Gear

As it is clear in Fig. 4.8, this designed and 3D printed partially geared helical gear is a multipurpose mechanical part. It is not fully geared as radial/ulnar motion of the wrist has a limited range of rotation so we don't need full gear here. It has also a place for sitting the bearing which is similar to the bottom of the bearing. There is also a groove in this part to hold the linear guide. This groove

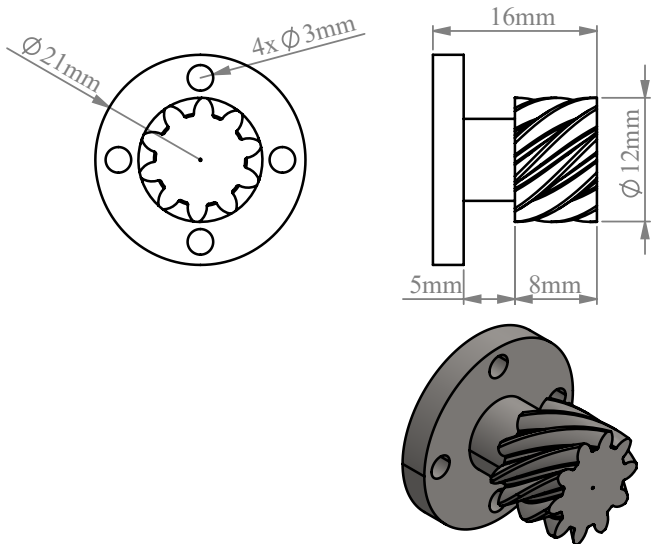

Figure 4.7: Pinion gear

shape is exactly similar to the linear guide cross-section.

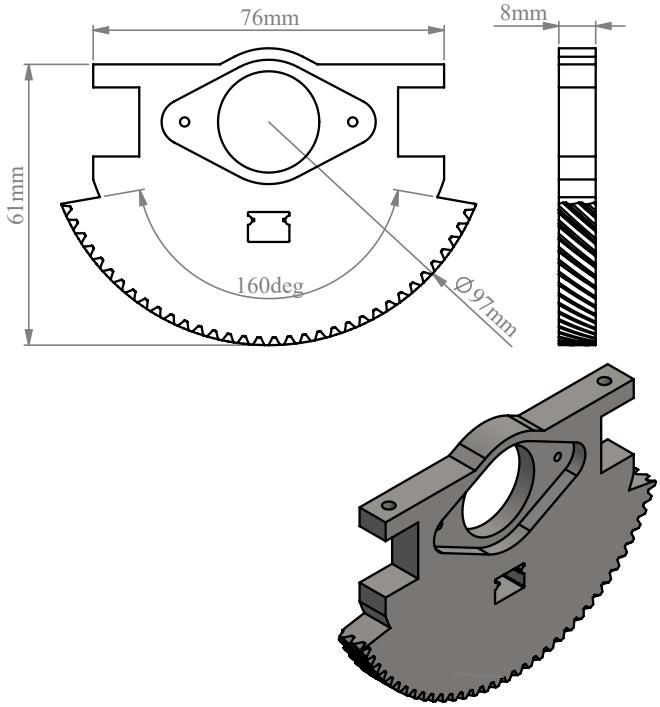

Figure 4.8: Helical gear

4.2.5 Bearing

Totally there are four flange type bearings in the robot structure which lead screw goes through all of them. Two of them are installed at each end of the rotating arm and allow the rotating arm to rotate around the lead screw axis and the other two are installed on the fixed bases of the robot at each end of the lead screw. These types of bearings are self-aligning and are able to compensate for any kind of misalignment. As the outer diameter of the lead screw is 8mm, the inner diameter of the selected bearings must be the same. So we chose the bearings blocks with the model number KFL08 which contain bearings with the model number 608RS. Fig. 4.9 demonstrates the bearing and its dimensions.

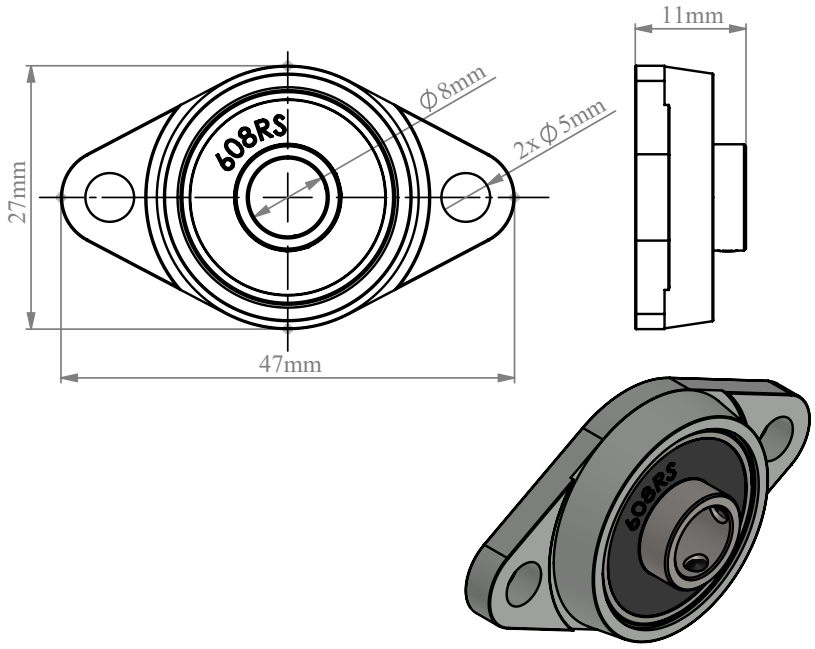

Figure 4.9: Bearing

4.2.6 Lead Screw and Nut

The lead screw length comes from the kinematic calculations in chapter 2. Also considering the limitations in the market, the minimum accessible length is 350mm which we chose for our application. We used the lead screw and nut of the ordinary 3D printers which can be easily found in the market. The pitch of the lead screw is 2mm and it has 4 flutes. With each rotation, the nut can

move 8mm along the lead screw axis. Fig. 4.10 and Fig. 4.11 show the details and dimensions of the lead screw and its nut.

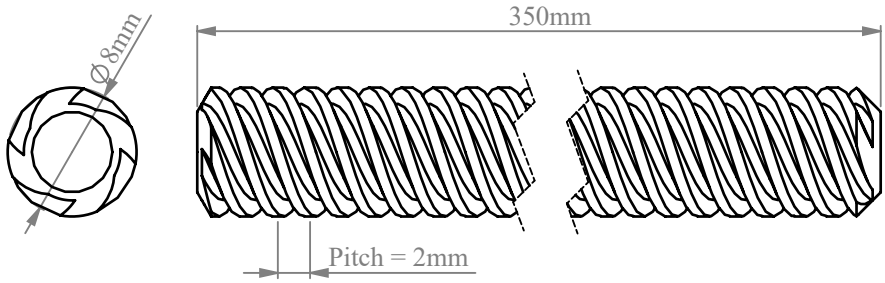

Figure 4.10: Lead screw

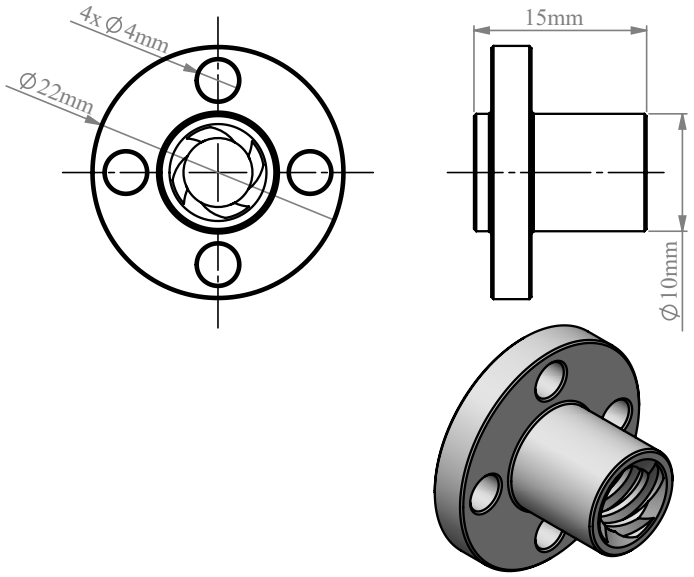

Figure 4.11: Nut

4.2.7 Linear Guide and Carriage

We used linear guide and carriage with MGN9 standard number which is used in the structure of many 3D printers and can be found in the market easily. The linear guide supports the nut and helps it move in a more straight line. It also helps us prevent the nut from rotating around the lead screw. So the nut will just go back and forth along the lead screw. You can see the details and dimensions of them in Fig. 4.12 and Fig. 4.13. The Linear guide is installed on the bottom of the rotating arm

with several screws.

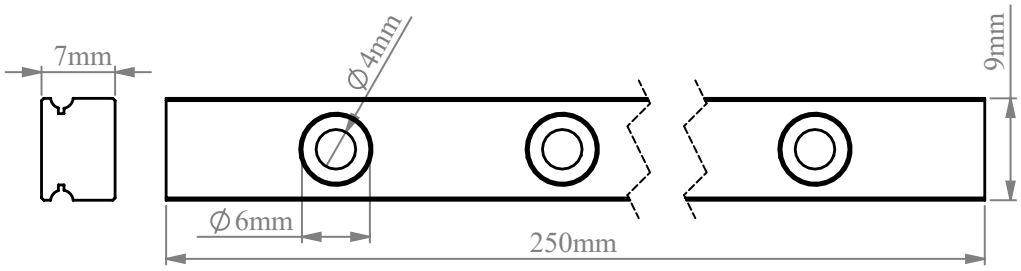

Figure 4.12: Linear guide

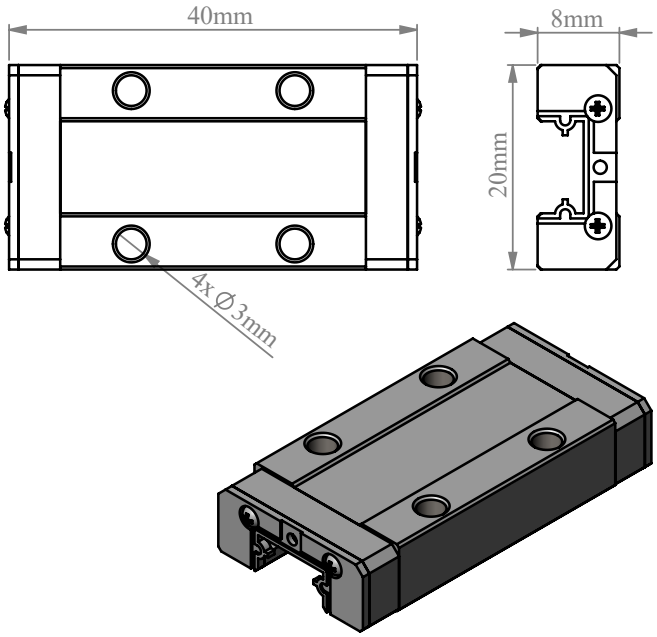

Figure 4.13: Carriage

4.2.8 Connection Part between the Carriage and Nut

Fig. 4.14 shows this designed and 3D printed part which from the bottom is connected to the carriage with four screws and from the front side is connected to the nut with another four screws. This part holds the nut and prevents it from rotating around the lead screw axis. So it makes the nut just have the linear motion along the lead screw axis.

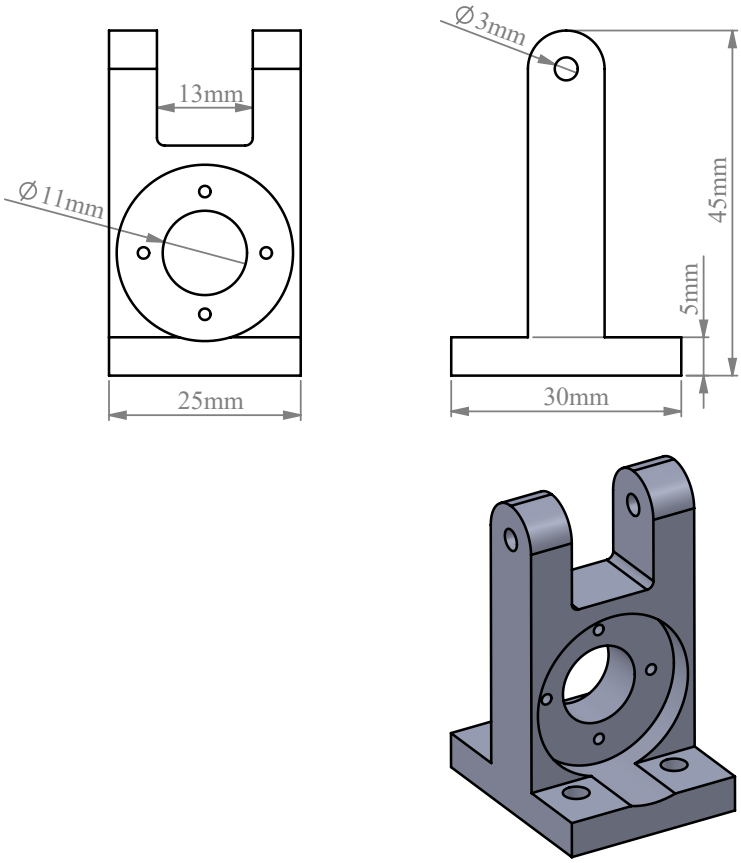

Figure 4.14: Connection part between the carriage and nut

4.2.9 Rotating Arm

The rotating arm is a 3D printed part that is a half-cylinder and has a groove for holding the rail. This part is rotated by the servo motor 2 through the pinion gear and helical gear. The whole parallelogram is connected to this part and it provides the ϕ rotation of the robot. This part and its details can be seen in Fig. 4.15.

4.2.10 Servo Motor

There are 2 servo motors in the robot. We Chose Dynamixel XL430-w250-T servo motor which is equipped with a gearbox and can provide enough torque for our application. the maximum torque which this servo motor can provide is 1.5 N.m. It has also an inner encoder for reading the position of the servo motor. This servo motor is cheap, each one less than fifty dollars. As its clear, servo

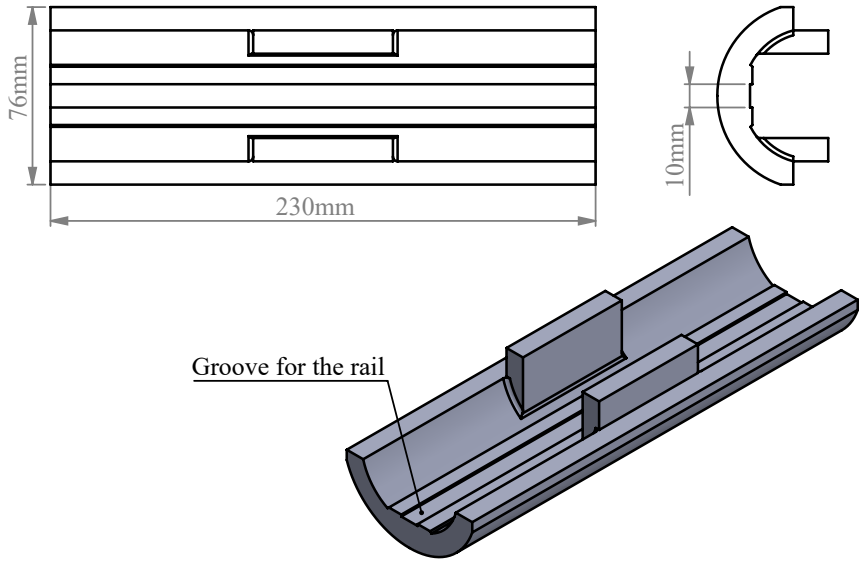

Figure 4.15: Rotating arm

motor 1 is under more pressure than servo motor 2 because it has to overcome the weight of the parallelogram and patient's hand together. Considering the maximum torque (1.1 N.m) generated by the designed trajectory in the human's wrist due to its weight and stiffness and also the torque generated by the weight of the parallelogram (0.2 N.m), the selected model of Dynamixel is a good choice for our application.

4.3 Fabrication

For manufacturing the robot links and most of the parts, we used the 3D printing method which is appropriate in our case as it is a fast, accessible and cheap method of production. We used a 3D printer named Ender 3 which is cheap and easily accessible in the market and uses filament materials. We used PLA filament as the 3D printing material which is cheap and lightweight and is easily accessible in the market. This method of production helps us to keep our robot cheap. We checked the dimensions of the 3d printed parts using a caliper to make sure that they are same as the designed dimensions. The error in all dimensions is less than 0.5 mm which is very good and acceptable. For 3d printing, we used a software named Cura which is an open source software. This software has many parameters that can be adjusted to reach the best quality of 3D-printed

parts. We set each layer height at 0.2 mm to have an excellent surface quality. As the PLA material shrinks after 3D printing, we have to consider the shrinkage factor of PLA, which is approximately 2 percent. It means that for 3D printing, we have to scale our models at 2 percent to reach the designed dimensions. The amount of torque exerted on the robot by the human hand is small, and the robot has a strong structure. For choosing the thickness of the robot links, we did a simple stress analysis in Solidworks software to check that the deformation of the 3D-printed parts is negligible. The links can tolerate the loads much more than the torque generated by the human hand.

4.4 Experimental Setup

The experimental setup includes four main parts which are explained in detail. As shown in Fig. 4.16, the first part is the robot itself which is installed vertically beside a table. The second part is a 12V DC power source which feeds the two servomotors of the robot. We can use batteries for feeding the servomotors too. The third part is a laptop which allows us to execute the codes of rehabilitation exercises and sending them to the servomotors. A micro controller can be used for controlling the robot too. The fourth part is an interface communication circuit named U2D2 which connects the laptop to the servomotors and allows transmitting and receiving of the data between the laptop and servomotors.

4.5 Testing Procedure

The robot was tested on one healthy person to check its ability in performing rehabilitation exercises. As it is demonstrated in Fig. 4.17, the healthy person is asked to sit on the chair and lay his hand on the table. For simulating the real situation, the person is asked to keep his hand's muscles relaxed as stroke patients have no muscle activity on one side of their bodies. The person is asked to grab the robot handle without exerting any force on it. Then by running the code through the laptop, the robot starts moving the person's hand and performing rehabilitation exercises. During the rehabilitation, the person is asked to keep calm and keep his muscles relaxed. The position data of the servo motors is read and stored for creating the graphs which were shown in the previous chapter.

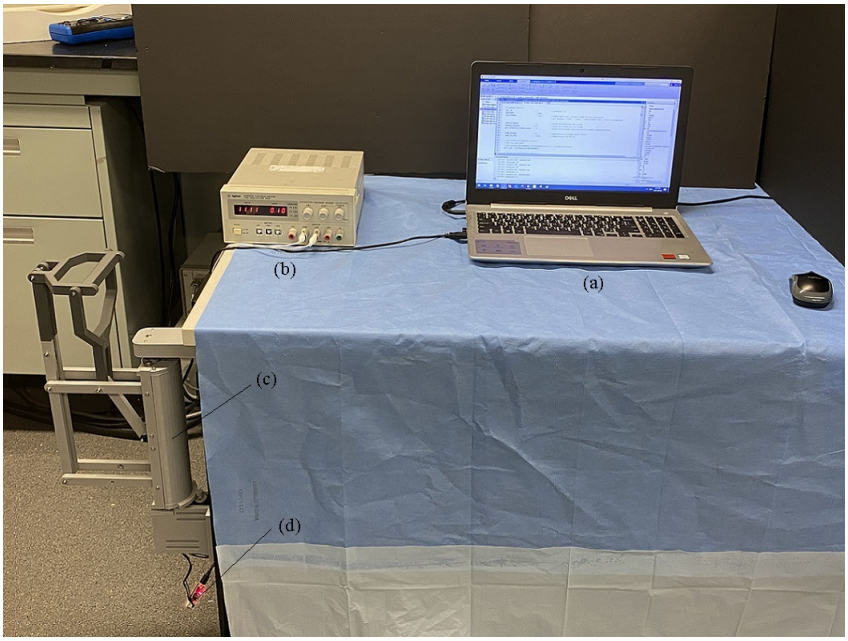

Figure 4.16: Experimental setup: (a) PC (b) 12V DC power source (c) rehabilitation robot (d) U2D2
.

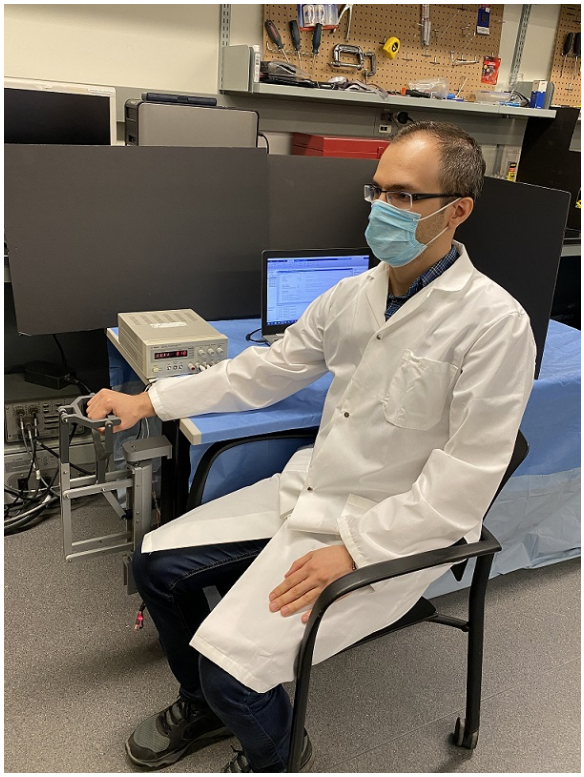

Figure 4.17: Testing the robot on a healthy person.

4.6 Summary

In this chapter, we presented the details of the robot and the designed mechanical parts used in the structure of the robot through different drawings. The manufacturing method and the material used for production were explained. Also the experimental setup and its different parts were shown and at last the procedure of the testing on one healthy person was explained in details.

Chapter 5

Conclusion and Future Work

In this thesis, a novel wrist rehabilitation robot called MOCH was introduced, which promises an affordable manufacturing method, portability, and compact size. An important part of the robot design was the development of a novel actuation system that enables us to place both actuators at the base, a feature which simplifies the robot structure, as well as reducing the problems with feeding wires to actuators on a rotating base. Experimental tests confirm the design requirements, and the robot prototype is reasonably priced and can be used by low-budget patients at home. Furthermore, it has acceptable tracking capability when it comes to passive wrist rehab exercises. we also described a novel approach for trajectory planning based on a dynamic model of the human wrist to make sure that applied torque on the human wrist during therapy is in the safe range to avoid any damages to the patient wrist.

Currently, MOCH is able to cover the passive wrist rehabilitation exercises. Our plan is to add a number of features to the robot to make it capable of doing active rehabilitation exercises, like adding a series elastic actuator to the robot structure as well as having a cable-driven capstan-drive instead of gear transition. These features will lead us to different control strategies like impedance and stiffness control which are necessary for active rehabilitation exercises. We also have in mind to equip the robot with a remote control which patient will be able to select several pre-defined trajectories. The robot also can be teleoperated by a professional therapist using a joystick. The robot end-effector has been designed based on the hand size of an average person. For the patients with different hand sizes, the RCM point of the mechanism may not exactly coincide on the wrist

center of rotation. So in the future we are going to design an end-effector with adjustable grasping handle. In the future, we are also going to check that the RCM point of the robot coincides the human wrist rotation center using cameras or 3D scanners. In the future, for the commercial product, we will do stress analysis using software like Ansys. Also, as the robot is under periodic loads, we will do fatigue analysis to ensure that the 3D-printed mechanical parts can resist.

Bibliography

[1] Johnson, C. O., Nguyen, M., Roth, G. A., Nichols, E., Alam, T., Abate, D., Abd-Allah, F., Abdelalim, A., Abraha, H. N., and Abu-Rmeileh, N. M., "Global, regional, and national burden of stroke, 1990–2016: a systematic analysis for the global burden of disease study 2016," *The Lancet Neurology*, vol. 18, no. 5, pp. 439–458, 2019.

[2] Dam, M., Tonin, P., Casson, S., Ermani, M., Pizzolato, G., Iaia, V., and Battistin, L., "The effects of long-term rehabilitation therapy on poststroke hemiplegic patients." *Stroke*, vol. 24, no. 8, pp. 1186–1191, 1993.

[3] Jørgensen, H. S., Nakayama, H., Raaschou, H. O., and Olsen, T. S., "Acute stroke care and rehabilitation: an analysis of the direct cost and its clinical and social determinants: the copenhagen stroke study," *Stroke*, vol. 28, no. 6, pp. 1138–1141, 1997.

[4] Zorowitz, R. D., Chen, E., Bianchini Tong, K., and Laouri, M., "Costs and rehabilitation use of stroke survivors: a retrospective study of medicare beneficiaries," *Topics in stroke rehabilitation*, vol. 16, no. 5, pp. 309–320, 2009.

[5] Hogan, N., Krebs, H. I., Charnnarong, J., Srikrishna, P., and Sharon, A., "Mit-manus: a workstation for manual therapy and training. i," *IEEE International Workshop on Robot and Human Communication*, pp. 161–165, 1992.

[6] Krebs, H. I., Volpe, B. T., Williams, D., Celestino, J., Charles, S. K., Lynch, D., and Hogan, N., "Robot-aided neurorehabilitation: a robot for wrist rehabilitation," *IEEE transactions on neural systems and rehabilitation engineering*, vol. 15, no. 3, pp. 327–335, 2007.

[7] Lum, P. S., Burgar, C. G., Kenney, D. E., and Van der Loos, H. M., "Quantification of force abnormalities during passive and active-assisted upper-limb reaching movements in post-stroke hemiparesis," *IEEE Transactions on Biomedical Engineering*, vol. 46, no. 6, pp. 652–662, 1999.

[8] Burgar, C. G., Lum, P. S., Shor, P. C., and Van der Loos, H. M., "Development of robots for rehabilitation therapy: The palo alto va/stanford experience," *Journal of rehabilitation research and development*, vol. 37, no. 6, pp. 663–674, 2000.

[9] Lum, P. S., Burgar, C. G., Van der Loos, M., Shor, P. C., Majmundar, M., and Yap, R., "The mime robotic system for upper-limb neuro-rehabilitation: results from a clinical trial in subacute stroke," *9th International Conference on Rehabilitation Robotics*, pp. 511–514, 2005.

[10] Reinkensmeyer, D. J., Takahashi, C. D., Timoszyk, W. K., Reinkensmeyer, A. N., and Kahn, L. E., "Design of robot assistance for arm movement therapy following stroke," *Advanced robotics*, vol. 14, no. 7, pp. 625–637, 2001.

[11] Reinkensmeyer, D. J., Kahn, L. E., Averbuch, M., McKenna-Cole, A., Schmit, B. D., and Rymer, W. Z., "Understanding and treating arm movement impairment after chronic brain injury: progress with the arm guide." *Journal of rehabilitation research and development*, vol. 37, no. 6, pp. 653–662, 2014.

[12] Nef, T. and Riener, R., "Armin-design of a novel arm rehabilitation robot," *9th International Conference on Rehabilitation Robotics (ICORR)*, pp. 57–60, 2005.

[13] Mihelj, M., Nef, T., and Riener, R., "Armin ii-7 dof rehabilitation robot: mechanics and kinematics," *IEEE International Conference on Robotics and Automation*, pp. 4120–4125, 2007.

[14] Hesse, S., Schmidt, H., Werner, C., and Bardeleben, A., "Upper and lower extremity robotic devices for rehabilitation and for studying motor control," *Current opinion in neurology*, vol. 16, no. 6, pp. 705–710, 2003.

[15] Hesse, S., Schmidt, H., and Werner, C., "Machines to support motor rehabilitation after stroke:

10 years of experience in berlin." *Journal of Rehabilitation Research & Development*, vol. 43, no. 5, 2006.

[16] Hesse, S., Schulte-Tigges, G., Konrad, M., Bardeleben, A., and Werner, C., "Robot-assisted arm trainer for the passive and active practice of bilateral forearm and wrist movements in hemiparetic subjects," *Archives of physical medicine and rehabilitation*, vol. 84, no. 6, pp. 915–920, 2003.

[17] Gupta, A., O'Malley, M. K., Patoglu, V., and Burgar, C., "Design, control and performance of ricewrist: a force feedback wrist exoskeleton for rehabilitation and training," *The International Journal of Robotics Research*, vol. 27, no. 2, pp. 233–251, 2008.

[18] Oblak, J., Cikajlo, I., and Matjačić, Z., "Universal haptic drive: A robot for arm and wrist rehabilitation," *IEEE Transactions on Neural Systems and Rehabilitation Engineering*, vol. 18, no. 3, pp. 293–302, 2009.

[19] Masia, L., Casadio, M., Sandini, G., and Morasso, P., "Eye-hand coordination during dynamic visuomotor rotations," *PloS one*, vol. 4, no. 9, p. e7004, 2009.

[20] Squeri, V., Masia, L., Giannoni, P., Sandini, G., and Morasso, P., "Wrist rehabilitation in chronic stroke patients by means of adaptive, progressive robot-aided therapy," *IEEE transactions on neural systems and rehabilitation engineering*, vol. 22, no. 2, pp. 312–325, 2013.

[21] Ren, Y., Kang, S. H., Park, H.-S., Wu, Y.-N., and Zhang, L.-Q., "Developing a multi-joint upper limb exoskeleton robot for diagnosis, therapy, and outcome evaluation in neurorehabilitation," *IEEE Transactions on Neural Systems and Rehabilitation Engineering*, vol. 21, no. 3, pp. 490–499, 2012.

[22] Martinez, J. A., Ng, P., Lu, S., Campagna, M. S., and Celik, O., "Design of wrist gimbal: A forearm and wrist exoskeleton for stroke rehabilitation," *IEEE 13th international conference on rehabilitation robotics (ICORR)*, pp. 1–6, 2013.

[23] Atlihan, M., Akdoğan, E., and Arslan, M. S., "Development of a therapeutic exercise robot for

wrist and forearm rehabilitation," *19th International Conference on Methods and Models in Automation and Robotics (MMAR)*, pp. 52–57, 2014.

[24] Akdoğan, E., Aktan, M. E., Koru, A. T., Arslan, M. S., Atlıhan, M., and Kuran, B., "Hybrid impedance control of a robot manipulator for wrist and forearm rehabilitation: Performance analysis and clinical results," *Mechatronics*, vol. 49, pp. 77–91, 2018.

[25] Cui, X., Chen, W., Agrawa, S. K., and Wang, J., "A novel customized cable-driven robot for 3-dof wrist and forearm motion training," *IEEE/RSJ International Conference on Intelligent Robots and Systems*, pp. 3579–3584, 2014.

[26] Chen, W., Cui, X., Zhang, J., and Wang, J., "A cable-driven wrist robotic rehabilitator using a novel torque-field controller for human motion training," *Review of Scientific Instruments*, vol. 86, no. 6, p. 065109, 2015.

[27] Khor, K., Chin, P., Hisyam, A., Yeong, C., Narayanan, A., and Su, E., "Development of cr2-haptic: A compact and portable rehabilitation robot for wrist and forearm training," *IEEE Conference on Biomedical Engineering and Sciences (IECBES)*, pp. 424–429, 2014.

[28] Khor, K. X., Chin, P. J. H., Yeong, C. F., Su, E. L. M., Narayanan, A. L. T., Rahman, H. A., and Khan, Q. I., "Portable and reconfigurable wrist robot improves hand function for post-stroke subjects," *IEEE Transactions on Neural Systems and Rehabilitation Engineering*, vol. 25, no. 10, pp. 1864–1873, 2017.

[29] Amirabdollahian, F., Ates, S., Basteris, A., Cesario, A., Buurke, J., Hermens, H., Hofs, D., Johansson, E., Mountain, G., and Nasr, N., "Design, development and deployment of a hand/wrist exoskeleton for home-based rehabilitation after stroke-script project," *Robotica*, vol. 32, no. 8, pp. 1331–1346, 2014.

[30] Bartlett, N. W., Lyau, V., Raiford, W. A., Holland, D., Gafford, J. B., Ellis, T. D., and Walsh, C. J., "A soft robotic orthosis for wrist rehabilitation," *Journal of Medical Devices*, vol. 9, no. 3, 2015.

[31] Rahman, M. H., Rahman, M. J., Cristobal, O., Saad, M., Kenné, J.-P., and Archambault, P. S., "Development of a whole arm wearable robotic exoskeleton for rehabilitation and to assist upper limb movements," *Robotica*, vol. 33, no. 1, pp. 19–39, 2015.

[32] Omarkulov, N., Telegenov, K., Zeinullin, M., Tursynbek, I., and Shintemirov, A., "Preliminary mechanical design of nu-wrist: A 3-dof self-aligning wrist rehabilitation robot," *6th IEEE International Conference on Biomedical Robotics and Biomechatronics (BioRob)*, pp. 962–967, 2016.

[33] Beom, J., Koh, S., Nam, H. S., Kim, W., Kim, Y., Seo, H. G., Oh, B.-M., Chung, S. G., and Kim, S., "Robotic mirror therapy system for functional recovery of hemiplegic arms," *Journal of visualized experiments: JoVE*, no. 114, 2016.

[34] Nam, H. S., Koh, S., Kim, Y. J., Beom, J., Lee, W. H., Lee, S.-U., and Kim, S., "Biomechanical reactions of exoskeleton neurorehabilitation robots in spastic elbows and wrists," *IEEE Transactions on Neural Systems and Rehabilitation Engineering*, vol. 25, no. 11, pp. 2196–2203, 2017.

[35] Higuma, T., Kiguchi, K., and Arata, J., "Low-profile two-degree-of-freedom wrist exoskeleton device using multiple spring blades," *IEEE Robotics and Automation Letters*, vol. 3, no. 1, pp. 305–311, 2017.

[36] Xu, D., Zhang, M., Sun, Y., Zhang, X., Xu, H., Li, Y., Li, X., and Xie, S. Q., "Development of a reconfigurable wrist rehabilitation device with an adaptive forearm holder," *IEEE/ASME International Conference on Advanced Intelligent Mechatronics (AIM)*, pp. 454–459, 2018.

[37] Xu, D., Zhang, M., Xu, H., Fu, J., Li, X., and Xie, S. Q., "Interactive compliance control of a wrist rehabilitation device (wred) with enhanced training safety," *Journal of healthcare engineering*, 2019.

[38] Buongiorno, D., Sotgiu, E., Leonardis, D., Marcheschi, S., Solazzi, M., and Frisoli, A., "Wres: a novel 3 dof wrist exoskeleton with tendon-driven differential transmission for neuro-rehabilitation and teleoperation," *IEEE Robotics and Automation Letters*, vol. 3, no. 3, pp. 2152–2159, 2018.

[39] Zhang, L., Li, J., Cui, Y., Dong, M., Fang, B., and Zhang, P., "Design and performance analysis of a parallel wrist rehabilitation robot (pwrr)," *Robotics and Autonomous Systems*, vol. 125, p. 103390, 2020.

[40] Huo, T., Yu, J., Zhao, H., Wu, H., and Zhang, Y., "A family of novel rcm rotational compliant mechanisms based on parasitic motion compensation," *Mechanism and Machine Theory*, vol. 156, p. 104168, 2021.

[41] Yang, Y., Liu, H., Zheng, H., Peng, Y., and Yu, Y., "Two types of remote-center-of-motion deployable manipulators with dual scissor-like mechanisms," *Mechanism and Machine Theory*, vol. 160, p. 104274, 2021.

[42] Wang, Z., Zhang, W., and Ding, X., "Design and analysis of a novel mechanism with a two-dof remote centre of motion," *Mechanism and Machine Theory*, vol. 153, p. 103990, 2020.

[43] Chen, G., Wang, J., Wang, H., Chen, C., Parenti-Castelli, V., and Angeles, J., "Design and validation of a spatial two-limb 3r1t parallel manipulator with remote center-of-motion," *Mechanism and Machine Theory*, vol. 149, p. 103807, 2020.

[44] Ryu, J., Cooney III, W. P., Askew, L. J., An, K.-N., and Chao, E. Y., "Functional ranges of motion of the wrist joint," *The Journal of hand surgery*, vol. 16, no. 3, pp. 409–419, 1991.

[45] Pando, A. L., Lee, H., Drake, W. B., Hogan, N., and Charles, S. K., "Position-dependent characterization of passive wrist stiffness," *IEEE Transactions on Biomedical Engineering*, vol. 61, no. 8, pp. 2235–2244, 2014.

[46] Charles, S. K. and Hogan, N., "Stiffness, not inertial coupling, determines path curvature of wrist motions," *Journal of neurophysiology*, vol. 107, no. 4, pp. 1230–1240, 2012.

[47] Molaei, A., Abedloo, E., Taghirad, H. D., and Marvi, Z., "Kinematic and workspace analysis of diamond: An innovative eye surgery robot," *23rd Iranian conference on electrical engineering*, pp. 882–887, 2015.

[48] Gosselin, C., "Kinematic analysis, optimization and programming of parallel robotic manipulators," 1988.

[49] Decostre, V., Canal, A., Ollivier, G., Ledoux, I., Moraux, A., Doppler, V., Payan, C. A. M., and Hogrel, J.-Y., "Wrist flexion and extension torques measured by highly sensitive dynamometer in healthy subjects from 5 to 80 years," *BMC musculoskeletal disorders*, vol. 16, no. 1, pp. 1–11, 2015.

[50] Dianat, I., Asadi, B., and Jafarabadi, M. A., "Wrist ulnar/radial torque strength measurements among iranian population: the effects of age, gender, body mass index and hand dominance," *Work*, vol. 53, no. 2, pp. 279–284, 2016.

[51] Williams, D. J., Krebs, H. I., and Hogan, N., "A robot for wrist rehabilitation," *Conference Proceedings of the 23rd Annual International Conference of the IEEE Engineering in Medicine and Biology Society*, vol. 2, pp. 1336–1339, 2001.

[52] Reinkensmeyer, D. J., Dewald, J. P., and Rymer, W. Z., "Guidance-based quantification of arm impairment following brain injury: a pilot study," *IEEE Transactions on Rehabilitation Engineering*, vol. 7, no. 1, pp. 1–11, 1999.

[53] Hussain, S., Jamwal, P. K., Van Vliet, P., and Ghayesh, M. H., "State-of-the-art robotic devices for wrist rehabilitation: Design and control aspects," *IEEE Transactions on Human-Machine Systems*, 2020.

[54] Taghirad, H. D., *Parallel robots: mechanics and control*. CRC press, 2013.

[55] Hogan, N., "Impedance control: An approach to manipulation," *American control conference*, pp. 304–313, 1984.

[56] Kelly, M., "An introduction to trajectory optimization: How to do your own direct collocation," *SIAM Review*, vol. 59, no. 4, pp. 849–904, 2017.